

AFDM-SCMA: A Promising Waveform for Massive Connectivity over High Mobility Channels

Qu Luo, *Graduate Student Member, IEEE*, Pei Xiao, *Senior Member, IEEE*, Zilong Liu, *Senior Member, IEEE*,
Ziwei Wan, *Graduate Student Member, IEEE*, Thomos, Nikolaos, *Senior Member, IEEE*,
Zhen Gao, *Member, IEEE*, and Ziming He, *Senior Member, IEEE*.

Abstract—This paper studies the affine frequency division multiplexing (AFDM)-empowered sparse code multiple access (SCMA) system, referred to as AFDM-SCMA, for supporting massive connectivity in high-mobility environments. First, by placing the sparse codewords on the AFDM chirp subcarriers, the input-output (I/O) relation of AFDM-SCMA systems is presented. Next, we delve into the generalized receiver design, chirp rate selection, and error rate performance of the proposed AFDM-SCMA. The proposed AFDM-SCMA is shown to provide a general framework and subsume the existing OFDM-SCMA as a special case. Third, for efficient transceiver design, we further propose a class of sparse codebooks for simplifying the I/O relation, referred to as I/O relation-inspired codebook design in this paper. Building upon these codebooks, we propose a novel iterative detection and decoding scheme with linear minimum mean square error (LMMSE) estimator for both downlink and uplink channels based on orthogonal approximate message passing principles. Our numerical results demonstrate the superiority of the proposed AFDM-SCMA systems over OFDM-SCMA systems in terms of the error rate performance. We show that the proposed receiver can significantly enhance the error rate performance while reducing the detection complexity.

Index Terms—Sparse code multiple access (SCMA), affine frequency division multiplexing (AFDM), chirp subcarrier, high-mobility channels, codebook design, orthogonal approximate message passing (OAMP), iterative detection and decoding.

I. INTRODUCTION

A. Background

IN recent years, there is a surging demand for wireless connectivity under various high mobility scenarios, e.g., integrated terrestrial and non-terrestrial networks, high-speed trains and vehicle-to-everything communications [1], [2]. In addition to the inter-symbol interference over multipath fading

channels, the communications in these high mobility scenarios could also suffer from the well-known time-varying channels with large Doppler [3]. In a low-earth orbit (LEO) satellite network, for instance, one needs to deal with time-varying high Doppler shift ranging from -48 KHz to $+48$ kHz for LEO altitude at 600 km above the earth and with carrier frequency of 2 GHz. The corresponding wireless channels are also called doubly selective channels. In this case, the widely deployed orthogonal frequency division multiplexing (OFDM) systems may be ineffective and unviable due to the significant inter-carrier interference (ICI) [3].

Against this background, affine frequency division multiplexing (AFDM) has emerged as an appealing solution for efficient and reliable communications over high-mobility channels [4]. The core idea of AFDM is built upon the discrete affine Fourier transform (DAFT) which was first introduced in [5]. Specifically, the proposed AFDM system employs quadratic exponential waveforms (i.e., chirp-modulated signals) as mutually orthogonal basis subcarriers (SCs). By contrast, OFDM systems rely on a set of orthogonal SCs whose phases grow linearly with their individual carrier frequency indexes. By appropriately tuning the chirp rate according to the Doppler profile of the channel, AFDM permits a separable and quasi-static channel representation, thus achieving to achieve the full diversity over the doubly selective channels. Moreover, every AFDM system is modulated/demodulated via inverse DAFT (IDAF)/DAFT, which is a generalization of many other important transforms, such as inverse discrete Fourier transform (IDFT)/DFT and inverse discrete Fresnel transform (IDFnT)/DFnT [6]. Notable examples include OFDM and orthogonal chirp division multiplexing (OCDM) [7], where IDFT/DFT and IDFnT/DFnT are utilized as the modulation/demodulation, respectively. More importantly, IDAF/DAFT can be efficiently implemented by leveraging OFDM modulation/demodulation with two one-tap filters [4]. These advantages of AFDM are attractive for its widespread applications in beyond-5G (B5G) wireless communication systems [8]–[10].

On the other hand, with the widespread proliferation of Internet-of-Things across every corner of this globe, new multiple access techniques with significantly improved spectrum efficiency are desired [11]. Over the past decade, non-orthogonal multiple access (NOMA) has attracted tremendous research attention due to its capability of supporting massive connectivity [11], [12]. By allowing overloaded transmission of multiple users, existing NOMA techniques can be mainly

Qu Luo and Pei Xiao are with the 5G & 6G Innovation Centre, University of Surrey, U. K. (email: {q.u.luo, p.xiao}@surrey.ac.uk).

Zilong Liu and Thomos, Nikolaos are with the School of Computer Science and Electronics Engineering, University of Essex, U. K. (email: {zilong.liu, nthomos}@essex.ac.uk).

Ziwei Wan and Zhen, Gao are with the School of Information and Electronics, Beijing Institute of Technology, Beijing 100081, China, and Ziwei Wan is also with the 5G & 6G Innovation Centre, University of Surrey, Guildford GU2 7XH, U. K. Zhen Gao is also with (BIT) Zhuhai 519088, China, also with the MIT Key Laboratory of Complex-Field Intelligent Sensing, BIT, Beijing 100081, China, also with the Advanced Technology Research Institute of BIT (Jinan), Jinan 250307, China, and also with the Yangtze Delta Region Academy, BIT (Jiaxing), Jiaxing 314019, China (E-mails: {gaozhen16, ziweiwang}@bit.edu.cn).

Ziming He is with the Samsung Cambridge Solution Centre, System LSI, Samsung Electronics, CB4 0DS Cambridge, U.K. (e-mail: ziming.he@samsung.com).

categorized into power-domain NOMA [13] and code-domain NOMA (CD-NOMA) [12]. Among many others, this paper is concerned with a disruptive CD-NOMA scheme, called sparse code multiple access (SCMA), which can achieve maximum-likelihood decoding performance with low complexity. Efficient message passing algorithm (MPA) [14] is adopted at the SCMA receiver to exploit the codebook sparsity as well as the multidimensional constellation shaping gain [15]–[17]. *The main aim of this work, therefore, is to study the integration of SCMA and AFDM for providing ultra-reliable massive connectivity in high mobility channels.*

B. Related Works

There has been a rich body of research works on SCMA, such as the peak-to-average power ratio reduction for OFDM-SCMA system [18], codebook design [19]–[23], and advanced receiver design [24], [25]. However, these works were mostly conducted under the assumption of static or low mobility scenarios. Very recently, NOMA transmissions building upon orthogonal time frequency space (OTFS) have been studied [26]–[30]. The basic idea of OTFS is to send the data over the delay-Doppler (DD) domain whereby every data symbol can enjoy the time-frequency diversity [31]. Although power-domain NOMA (PD-NOMA) has been integrated with OTFS in [28], [32], the resultant systems require delicate user grouping and power allocation. Compared to SCMA, these might be challenging in high mobility channels due to small channel coherence time. Moreover, as shown in [12], SCMA enjoys high signal space diversity and hence outperforms power-domain NOMA in terms of the error performance. By integrating SCMA with OTFS, it was shown in [28] that OTFS-SCMA provides improved error performance than conventional OFDM-SCMA and OTFS-aided PD-NOMA. However, their proposed two-stage detector consisting of a linear minimum mean square error (LMMSE) detector and MPA in downlink channels prevents the exploitation of the full potential of OTFS-SCMA system [27]. To further enhance the error performance, an iterative structure between the LMMSE and MPA based on the orthogonal approximate messaging passing (OAMP) principles was developed in [27], yet at the price of a high computational complexity. [26] studied an SCMA empowered coordinated multi-point vehicle communication system, where multiple mobile users are allowed to share the same DD resources with OTFS. However, as OTFS suffers from the high complexity of implementation and excessive pilot overhead due to its 2D structure, the OTFS aided SCMA systems also face these challenges.

The study of AFDM is still at its early stage. The performance of AFDM for high frequency band communication impaired with CFO and phase noise was evaluated in [33]. Recently, [8] studied the orthogonal resource allocation, channel estimation and multi-user access scheme for the AFDM with multiple-input multiple-output in high mobility scenarios. [34], [35] studied the index modulation empowered AFDM schemes for enhancing system spectrum efficiency. A generalized MPA-based detection scheme was developed in [36] to exploit the channel sparsity in AFDM systems. However, the MPA complexity grows exponentially as the number of

multipaths increases. In [37], instead of using DAFT, a DFT-based modulation and demodulation techniques for AFDM was introduced, making AFDM backward compliant with the OFDM systems. Moreover, AFDM was also explored for integrated sensing and communications in [9], [10]. Moreover, AFDM enjoys high backward compatibility with OFDM due to its 1D modulation nature instead of the 2D linear transform in OTFS. This leads to reduced implementation complexity and channel estimation overhead compared to OTFS [4], [8].

C. Motivation and contributions

While the above works have revealed the superiority of AFDM, how it can enable improved massive connectivity over high mobility channels remains largely open. Our primary objective is to study a novel SCMA empowered AFDM system, referred to as the AFDM-SCMA. Different from existing works [26]–[28] that primarily address uncoded systems, our focus is on coded systems. The design of AFDM-SCMA system is challenging due to the following reasons: 1) in AFDM-SCMA systems, as different SCMA users may experience different radio propagation channels, the AFDM parameters, such as the chirp rate, should be carefully tuned to attain full diversity; 2) Albeit there are numerous SCMA codebooks reported in the literature, they are not optimized for AFDM-SCMA systems; and 3) the MPA might not be applicable to AFDM-SCMA because its complexity grows exponentially with the number of multipaths.

The main contributions of this work are summarized as follows:

- We propose a novel AFDM-SCMA system for supporting massive connectivity in high mobility environments. The proposed approach begins with the allocation of SCMA codewords to AFDM SCs. Then, the system model for both downlink and uplink AFDM-SCMA systems are given, followed by a generalized multi-user detection design.
- We then delve into an analysis of the bit error rate (BER) performance of the AFDM-SCMA systems. In contrast to the BER analyses in the existing OFDM-SCMA systems, where every SC is assumed to be independent and identically distributed, we address a more realistic scenario involving multipath fading channels. In addition, to attain large diversity gain, the system parameters, such as the chirp rate, in AFDM-SCMA are also studied.
- We propose a class of sparse codebooks for simplifying the input-output (i.e., I/O) relation in AFDM-SCMA systems, referred to as I/O relation-inspired codebook design. Building upon these codebooks, we introduce a novel iterative detection and decoding scheme for both downlink and uplink channels based on the OAMP principles. Notably, the proposed receiver eliminates the need for an MPA decoder, resulting in a substantial reduction in decoding complexity in comparison to the two-stage receiver proposed in previous works [27], [28].
- Our numerical results demonstrate the superiority of the proposed AFDM-SCMA systems. The results show that: 1) the proposed AFDM-SCMA significantly outperforms OFDM-SCMA over doubly selective channels; 2) the

derived analytical BER curves match well with the simulated ones; 3) the proposed transceiver design can significantly enhance the BER performance with reduced the decoding complexity; and 4) the proposed I/O codebook and OAMP-assisted receiver can also be employed for OTFS-SCMA systems for performance enhancement and low-complexity detection.

D. Organization

This paper is organized as follows: Section II describes the preliminary concepts about SCMA and AFDM. The proposed AFDM-SCMA is presented in Section III, where the comprehensive details on the signal model, receiver design, AFDM-SCMA parameters, and an in-depth analysis of the BER performance are provided. Section IV introduces the proposed I/O relation-inspired codebook design and the proposed advanced iterative detection and decoding scheme. The simulation results are presented and analyzed in Section V. Section VI concludes the paper.

E. Notation

The n -dimensional complex, real and binary vector spaces are denoted as \mathbb{C}^n , \mathbb{R}^n and \mathbb{B}^n , respectively. Similarly, $\mathbb{C}^{k \times n}$, $\mathbb{R}^{k \times n}$ and $\mathbb{B}^{k \times n}$ denote the $(k \times n)$ -dimensional complex, real and binary matrix spaces, respectively. \mathbf{I}_n denotes an $n \times n$ -dimensional identity matrix. $\text{diag}(\mathbf{x})$ gives a diagonal matrix with the diagonal vector of \mathbf{x} . $(\cdot)^T$ and $(\cdot)^H$ denote the transpose and the Hermitian transpose operation, respectively.

II. PRELIMINARIES

A. SCMA

Consider a $K \times J$ SCMA system, where J users communicate over K resource nodes (RNs). The overloading factor of SCMA system is defined by $\xi = J/K > 100\%$, indicating that the number of users that concurrently communicate is larger than the total number of orthogonal resources. Each user is assigned a unique codebook, denoted by $\mathcal{X}_j = [\mathbf{x}_{j,1}, \mathbf{x}_{j,2}, \dots, \mathbf{x}_{j,M}] \in \mathbb{C}^{K \times M}$, $j \in \{1, 2, \dots, J\}$, where M denotes the codebook size and $\mathbf{x}_{j,m}$ is the m th codeword with a dimension of K . The average codeword power of a codebook is assumed to be unit, i.e., $\text{Tr}(\mathcal{X}_j^H \mathcal{X}_j) = M$. During the transmission, each user selects one codeword based on the input binary message. Denote $\mathbf{b}_j = [b_{j,1}, b_{j,2}, \dots, b_{j,\log_2 M}]^T \in \mathbb{B}^{\log_2 M \times 1}$ by the input binary message of the j th user. The SCMA encoding process of j th user can be expressed as [21]

$$f_j : \mathbb{B}^{\log_2 M \times 1} \rightarrow \mathcal{X}_j \in \mathbb{C}^{K \times M}, \text{ i.e., } \mathbf{x}_j = f_j(\mathbf{b}_j). \quad (1)$$

In SCMA, the codebook sparsity is exploited by MPA for low-complexity decoding. Each K -dimensional complex codeword has only V non-zero elements, and the sparsity of the J codebooks is reflected by the sparse indicator matrix $\mathbf{F}_{K \times J} \in \mathbb{B}^{K \times J}$. An element of \mathbf{F} is defined as $f_{k,j}$ which takes the value of 1 if and only if the k th resource is occupied by the j th user, and 0 otherwise. A factor graph can graphically represents the sharing of the resources among multiple users. Specifically, the factor graph of a $K \times J$ SCMA system contains J user nodes (UNs) and K RNs. The j th UN is

connected to the k th RN only if it occupies the k th resource. In addition, the number of users collides over a RN is denoted as d_f . In this paper, the following indicator matrix $J = 6$, $K = 4$, $d_f = 3$ and $V = 2$ is considered [21]:

$$\mathbf{F}_{4 \times 6} = \begin{bmatrix} 0 & 1 & 1 & 0 & 1 & 0 \\ 1 & 0 & 1 & 0 & 0 & 1 \\ 0 & 1 & 0 & 1 & 0 & 1 \\ 1 & 0 & 0 & 1 & 1 & 0 \end{bmatrix}, \quad (2)$$

where the factor graph representation is shown in Fig. 2.

1) *Downlink channels*: In downlink transmissions, the codewords of J users are superimposed on K RNs at the base station (BS), i.e., [21]

$$\mathbf{w} = \sum_{j=1}^J \mathbf{x}_j, \quad (3)$$

where $\mathbf{w} = [w_1, w_2, \dots, w_K]^T \in \mathbb{C}^{K \times 1}$ is the superimposed codeword. The received signal $\mathbf{y}_u = [y_{u,1}, \dots, y_{u,K}]^T$ at the u th user can be expressed as

$$\mathbf{y}_u = \text{diag}(\mathbf{h}_u) \mathbf{w} + \mathbf{n}_u, \quad (4)$$

where $\mathbf{h}_u = [h_{u,1}, h_{u,2}, \dots, h_{u,K}]^T$ is the channel gain between the BS and the u th user and \mathbf{n}_u is the Gaussian noise vector that has $\mathcal{CN}(0, N_0)$ entries, where N_0 is the noise variance. For simplicity, the subscript u is omitted throughout this paper.

2) *Uplink channels*: In contrast, for the uplink transmission, the $K \times 1$ received signal vector \mathbf{r} at the BS can be written as

$$\mathbf{r} = \sum_{j=1}^J \text{diag}(\mathbf{g}_j) \mathbf{x}_j + \mathbf{n}, \quad (5)$$

where $\mathbf{g}_j = [g_{j,1}, g_{j,2}, \dots, g_{j,K}]^T$ denotes the channel vector from the j th user and \mathbf{n} the Gaussian noise vector at the BS which consists of K entries each subject to independent $\mathcal{CN}(0, N_0)$ distribution.

B. AFDM

This subsection first introduces the digital implementation of AFDM and then presents the I/O relation. For ease of presentation, notations \mathbf{x} , \mathbf{y} and \mathbf{r} are reused to describe the signal model of AFDM in this subsection.

1) *AFDM modulation*: Denote $\mathbf{x} \in \mathbb{C}^{N \times 1}$ by the transmitted vector in the DAFT domain, then the modulated symbol is obtained by taking the IDAFT of \mathbf{x} , i.e.,

$$s[n] = \sum_{m=0}^{N-1} x[m] \varphi_n(m), n = 0, 1, \dots, N-1, \quad (6)$$

where $\varphi_n(m)$ is the AFT kernel at the m -th SC and associated to the n -th modulated symbol. Specifically, we have

$$\varphi_n(m) = \frac{1}{\sqrt{N}} e^{j2\pi(c_1 n^2 + c_2 m^2 + \frac{nm}{N})}, \quad (7)$$

where $c_1 \geq 0$ and $c_2 \geq 0$ are the AFDM parameters. Note that (6) can be written in the matrix form as

$$\mathbf{s} = \Lambda_{c_1}^H \mathbf{F}^H \Lambda_{c_2}^H \mathbf{x} = \mathbf{A}^H \mathbf{x}, \quad (8)$$

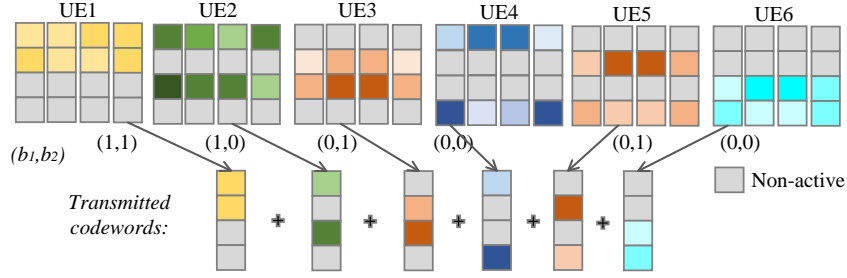


Fig. 1: An example of SCMA encoding.

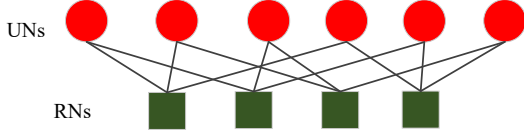


Fig. 2: Factor graph representation of the SCMA system in (2).

where $\mathbf{A} = \Lambda_{c_2} \mathbf{F} \Lambda_{c_1}$ is the DAFT matrix, $\Lambda_c = \text{diag}(e^{-j2\pi cn^2}, n = 0, 1, \dots, N-1)$, and \mathbf{F} is the DFT matrix with entries $e^{-j2\pi mn/N}/\sqrt{N}$.

In an AFDM system, a prefix is required for combating multipath propagation and converting linear convolution into circulant convolution. Different from OFDM, in which a cyclic prefix (CP) is utilized, AFDM employs a chirp-periodic prefix (CPP) due to the inherent periodicity of DAFT. The CPP with length of N_{CPP} is given by

$$s[n] = s[N+n]e^{-j2\pi c_1(N^2+2Nn)}, n = -N_{\text{CPP}}, \dots, -1. \quad (9)$$

2) *Channel*: We consider a doubly selective channel with the channel response at time n and delay l given by

$$g_n(l) = \sum_{p=1}^P h_p e^{-j\frac{2\pi}{N}\nu_p n} \delta(l - l_p), \quad (10)$$

where P is the number of paths, and h_p , ν_p and l_p are the channel gain, Doppler shift and the integer delay of the p th path. Note that ν_p is normalized with respect to the SC spacing and can be expressed as $\nu_p = \alpha_p + \beta_p$, where $\alpha_p \in [-\alpha_{\text{max}}, -\alpha_{\text{max}} + 1, \dots, \alpha_{\text{max}}]$ and $\beta_p \in (-\frac{1}{2}, \frac{1}{2}]$ denotes the integer and fractional parts of ν_i , respectively, and α_{max} is the maximum integer Doppler.

3) *AFDM demodulation*: At the receiver side, the received time domain signal can be expressed as

$$r[n] = \sum_{l=0}^{\infty} s[n-p]g_n[l] + v[n], \quad (11)$$

where $v[n] \sim \mathcal{CN}(0, N_0)$ is the additive Gaussian noise. After discarding the CPP, (11) can be re-written in the matrix form as

$$\mathbf{r} = \sum_{p=0}^P \mathbf{H}_p \mathbf{s} + \mathbf{v}, \quad (12)$$

where \mathbf{v} is the noise vector in the time domain, $\mathbf{H}_p = h_p \mathbf{\Gamma}_{\text{CPP}_p} \mathbf{\Delta}_{\nu_p} \mathbf{\Pi}^{l_p}$ is the time domain channel matrix of the p th path, $\mathbf{\Pi}$ denotes the forward cyclic-shift matrix, i.e.,

$$\mathbf{\Pi} = \begin{bmatrix} 0 & \dots & 0 & 1 \\ 1 & \dots & 0 & 0 \\ \vdots & \ddots & \ddots & \vdots \\ 0 & \dots & 1 & 0 \end{bmatrix}_{N \times N}, \quad (13)$$

$\mathbf{\Delta}_{\nu_p} = \text{diag}(e^{-j\frac{2\pi}{N}\nu_p n}, n = 0, 1, \dots, N-1)$ models the Doppler effect, and the effective CPP matrix $\mathbf{\Gamma}_{\text{CPP}_p}$ takes the following expression

$$\mathbf{\Gamma}_{\text{CPP}_p} = \text{diag}\left(\begin{cases} e^{-j2\pi c_1(N^2-2N(l_p-n))}, & n < l_p, \\ 1, & n \geq l_p, \end{cases}\right). \quad (14)$$

Finally, the received signal in the DAFT domain is obtained by applying the DAFT transform, i.e.,

$$\mathbf{y} = \Lambda_{c_2} \mathbf{F} \Lambda_{c_1} \mathbf{r} = \mathbf{A} \mathbf{r}. \quad (15)$$

4) *The I/O relation*: Substituting (6), (10) and (11) into (15), one has the I/O relation in the time domain given by

$$y[n] = \frac{1}{N} \sum_{m=0}^{N-1} \sum_{p=1}^P h_p \eta(l_p, n, m) \gamma(l_p, \nu_p, n, m) x[m] + v[n], \quad (16)$$

where

$$\eta(l_p, n, m) = e^{j\frac{2\pi}{N}(Nc_1 l_p^2 - ml_p + Nc_2(m^2 - n^2))}, \quad (17a)$$

$$\gamma(l_p, \nu_p, n, m) = \frac{e^{-j2\pi(n-m+\text{Ind}_p+\beta_p)} - 1}{e^{-j\frac{2\pi}{N}(n-m+\text{Ind}_p+\beta_p)} - 1}, \quad (17b)$$

where $\text{Ind}_p = (\alpha_p + 2Nc_1 l_p)_N$. The I/O relation in the DAFT domain in the matrix form is given by

$$\begin{aligned} \mathbf{y} &= \sum_{p=1}^P h_i \underbrace{\Lambda_{c_2} \mathbf{F} \Lambda_{c_1} \mathbf{\Gamma}_{\text{CPP}_p} \mathbf{\Delta}_{\nu_p} \mathbf{\Pi}^{l_p} \Lambda_{c_1}^H \mathbf{F}^H \Lambda_{c_2}^H}_{\mathbf{H}_p} \mathbf{x} + \tilde{\mathbf{v}} \\ &= \mathbf{H}_{\text{eff}} \mathbf{x} + \tilde{\mathbf{v}}, \end{aligned} \quad (18)$$

where $\mathbf{H}_{\text{eff}} = \sum_{p=1}^P h_p \mathbf{H}_p$ is the effective channel matrix and $\tilde{\mathbf{v}}$ is the noise vector with the same distribution of \mathbf{v} as \mathbf{A} is a unitary matrix. It can be shown that the element of \mathbf{H}_p at row n and column m is

$$\mathbf{H}_p[n, m] = \eta(l_p, n, m) \gamma(l_p, \nu_p, n, m). \quad (19)$$

In AFDM systems, the parameters c_1 and c_2 can be adjusted so that the non-zero elements of matrix \mathbf{H}_p in each path do not overlap within \mathbf{H}_{eff} , resulting in a comprehensive delay-Doppler channel representation. Further insights into the channel representation will be provided in the subsequent section in conjunction with the SCMA structure.

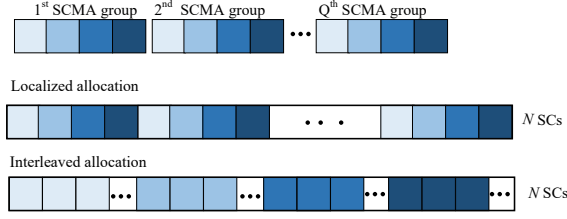


Fig. 3: SCMA codewords allocation.

III. PROPOSED AFDM-SCMA

In this section, we present the proposed AFDM-SCMA framework for both downlink and uplink channels. We start by introducing the codeword allocation within AFDM-SCMA systems. Subsequently, we delve into the signal models and the design of multi-user detection for the proposed AFDM-SCMA schemes. Furthermore, the selection of the AFDM-SCMA system parameters and an in-depth analysis of the performance of AFDM-SCMA are also presented.

A. SCMA Codewords Allocation

In AFDM-SCMA, multiple SCMA groups with each group consisting of K RNs and J UNs are transmitted over N AFDM SCs. In this paper, we consider Q SCMA groups that serve J users and assume that $N = QK$. Denote $\mathbf{x}_{j,q}$ by the q th SCMA codewords of user j . Let $\bar{\mathbf{x}}_{\text{sym},j}$ consists of all the SCMA codewords to be allocated to the AFDM SCs, which takes the following expression:

$$\bar{\mathbf{x}}_{\text{sym},j} = [\mathbf{x}_{j,1}^T, \mathbf{x}_{j,2}^T, \dots, \mathbf{x}_{j,Q}^T]^T. \quad (20)$$

We further denote $\mathbf{x}_{\text{sym},j}$ by the transmitted vector after the codewords allocation. To assign the SCMA codewords to the AFDM SCs, we consider the following two distinct allocation schemes, as depicted in Fig. 3, which discuss next.

a) *Localized allocation*: The N AFDM SCs are partitioned into $Q = N/K$ groups, with each group consisting of K SCs. Then, the i th SCMA codeword, i.e., $\mathbf{x}_{j,q}^T, j = 1, 2, \dots, J$, is consecutively mapped to the q th AFDM group.

b) *Interleaved allocation*: The N AFDM SCs are divided into K groups, each consisting of Q SCs. The k th entry of $\mathbf{x}_{j,q}$ is transmitted at the q th position of group k over the corresponding AFDM SC.

B. Downlink AFDM-SCMA

The proposed downlink AFDM-SCMA system is presented in Fig. 4. The BS superimposes the symbol vectors of all users and performs codeword allocations, leading to the superimposed codeword vector as

$$\mathbf{w}_{\text{sym}} = \sum_{j=1}^J \mathbf{x}_{\text{sym},j}. \quad (21)$$

Invoking the I/O relation of the AFDM system, the received signal in the DAFT domain, denoted by $\mathbf{y}_{\text{sym}} \in \mathbb{C}^{N \times 1}$, can be written as

$$\mathbf{y}_{\text{sym}} = \mathbf{H}_{\text{sym}} \mathbf{w}_{\text{sym}} + \mathbf{v}_{\text{sym}}, \quad (22)$$

where $\mathbf{v}_{\text{sym}} \in \mathbb{C}^{N \times 1}$ is the complex Gaussian noise vector with zero mean and variance of $\mathbf{I}_N N_0$, and $\mathbf{H}_{\text{sym}} \in \mathbb{C}^{N \times N}$

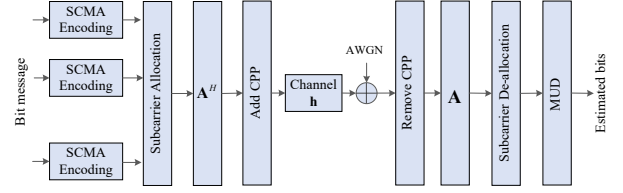


Fig. 4: The proposed downlink AFDM-SCMA system.

denotes the complex channel coefficient matrix specifying the relationship defined in (18).

As evident from (21) and (22) that \mathbf{w}_{sym} can be recovered from \mathbf{y}_{sym} by applying a simple LMMSE-based detector, i.e.,

$$\hat{\mathbf{w}}_{\text{sum}} = \mathbf{H}_{\text{sym}}^H [\mathbf{H}_{\text{sym}} \mathbf{H}_{\text{sym}}^H + N_0^2 \mathbf{I}_N]^{-1} \mathbf{y}_{\text{sym}}. \quad (23)$$

Subsequently, the estimated $\hat{\mathbf{w}}_{\text{sum}}$ will be fed to a standard MPA decoder to obtain the detected SCMA codewords $\hat{\mathbf{x}}_{\text{sym},j}, j = 1, 2, \dots, J$.

Remark 1: The above detection process is referred to as a two-stage detection scheme, similar to the one in [28]. It is worth noting that such a scheme has a considerably high computational complexity. In Section IV, we will show that the detection can be simplified to an one-stage LMMSE-based detector by joint design of efficient sparse codebooks and advanced iterative detection and decoding.

C. Uplink AFDM-SCMA

Consider an uplink AFDM-SCMA system with J users communicate over N AFDM SCs. At the transmitter side, each user performs independent AFDM modulation with the same AFDM parameters (c_1, c_2). At the BS, the received signal after AFDM demodulation, denoted by $\mathbf{r}_{\text{sym}} \in \mathbb{C}^{N \times 1}$, is given by

$$\begin{aligned} \mathbf{r}_{\text{sym}} &= \sum_{j=1}^J \mathbf{G}_{\text{sym},j} \mathbf{x}_{\text{sym},j} + \mathbf{n}_{\text{sym}} \\ &= \mathbf{G}_{\text{all}} \mathbf{x}_{\text{all}} + \mathbf{n}_{\text{sym}}, \end{aligned} \quad (24)$$

where $\mathbf{G}_{\text{sym},j} \in \mathbb{C}^{N \times N}$ denotes the effective channel matrix between the j th user and the BS, $\mathbf{n}_{\text{sym}} \in \mathbb{C}^{N \times 1}$ denotes the complex Gaussian noise vector with zero mean and variance of $\mathbf{I}_N N_0$, and

$$\begin{aligned} \mathbf{G}_{\text{all}} &= [\mathbf{G}_{\text{sym},1}, \mathbf{G}_{\text{sym},2}, \dots, \mathbf{G}_{\text{sym},J}] \in \mathbb{C}^{N \times NJ}, \\ \mathbf{x}_{\text{all}} &= [\mathbf{x}_{\text{sym},1}^T, \mathbf{x}_{\text{sym},2}^T, \dots, \mathbf{x}_{\text{sym},J}^T]^T \in \mathbb{C}^{NJ \times 1}. \end{aligned} \quad (25)$$

Note that \mathbf{G}_{all} and \mathbf{x}_{all} are sparse vectors. Hence, a generalized MPA detector can be utilized for uplink AFDM-SCMA system. Denote $x_{\text{all},m}$ by the m th codeword in \mathbf{x}_{all} . Let $\Omega_{\mathbf{G}_{\text{all}}}(n)$ be the set of the columns at the n th row of \mathbf{G}_{all} connecting to the transmitted codeword $x_{\text{all},m}$. In MPA, the major challenge is to compute the belief message from the observation nodes to the variable nodes. In AFDM-SCMA systems, assume that the belief message from the codeword node m towards the observation node n is denoted by $I_{c_m \rightarrow r_n}(x_{\text{all},m})$, then based

on the sum-product rule, the message propagating from r_n to c_m is computed as follows [17]:

$$I_{r_n \rightarrow c_m}(x_{\text{all},m}) = \sum_{\substack{x_{\text{all},m'}, \\ m' \in \Omega_{\mathbf{G}_{\text{all}}(n)} \setminus \{m\}}} \frac{1}{\sqrt{2\pi N_0}} \exp \left\{ -\frac{1}{2N_0} \left| r_n - \sum_{m \in \Omega_{\mathbf{G}_{\text{all}}(n)}} g_{n,m} x_{\text{all},m} \right|^2 \right\} \times \prod_{m' \in \Omega_{\mathbf{G}_{\text{all}}(n)} \setminus \{m\}} I_{c_{m'} \rightarrow r_n}(x_{\text{all},m'}). \quad (26)$$

Due to the limited space, the update rule of $I_{c_{m'} \rightarrow r_n}(x_{\text{all},m'})$ is omitted in this paper. The readers are referred to [38] for more details about MPA. The computational complexity of MPA-based detector can be approximated as $\mathcal{O}(M^{|\Omega_{\mathbf{G}_{\text{all}}(n)}|})$.

Remark 2: The number of nonzero entries at the n th row of \mathbf{G}_{all} , i.e., $|\Omega_{\mathbf{G}_{\text{all}}(n)}|$, is determined by the number of paths and the number of users that share the same SCMA RN. For integer Doppler, we have $|\Omega_{\mathbf{G}_{\text{all}}(n)}| = d_f P$, where d_f is the number of non-zero entries at each row of \mathbf{F} . Obviously, the detection complexity increases exponentially with the increase of P and d_f . To this end, low complexity detection and decoding is further proposed in Section IV.

D. AFDM-SCMA Parameters

The performance of DAFT-based modulation schemes heavily depends on the choice of parameters c_1 and c_2 . Recall (19), for each path, $\eta(l_p, n, m)$ has unit energy, and $\gamma(l_p, \nu_p, n, m)$ achieves the peak energy at $m = (n + \text{Ind}_p)_N$ and decreases as m moves away from $(n + \text{Ind}_p)_N$. In this paper, we consider $\gamma(l_p, \nu_p, n, m)$ is non-zero only for m moves k_ν away from $(m + \text{Ind}_p)_N$. Namely, the following holds

$$|\mathbf{H}_p[n, m]| = \begin{cases} |\gamma(l_p, \nu_p, n, m)| & (n + \text{Ind}_p - k_\nu)_N \leq m \leq (n + \text{Ind}_p + k_\nu)_N \\ 0 & \text{otherwise} \end{cases}. \quad (27)$$

Fig. 5 shows an example of the effective channel matrix of a downlink AFDM-SCMA system over a two-path channel. As evident from (27), the location of each path depends on its delay-Doppler information and AFDM parameters. It is essential to determine values for c_1 and c_2 as such the DAFT domain impulse response forms a full delay-Doppler representation of the channel. In addition, c_1 and c_2 should also be adjusted to achieve the best diversity gain of AFDM-SCMA in doubly selective channels. Denote l_p^j and $\nu_p^j = \alpha_p^j + \beta_p^j$ by the delay and the normalized Doppler of the p th path of the j th user, respectively, where

$$\alpha_p^j \in [-\alpha_{\text{max}}, -\alpha_{\text{max}} + 1, \dots, \alpha_{\text{max}}], \quad (28)$$

$$\beta_p^j \in \left(-\frac{1}{2}, \frac{1}{2}\right], j = 1, 2, \dots, J.$$

The number of paths for each user is denoted by P_j . For the j th user, to achieve a large diversity gain, the positions of non-zero entries in the channel matrix for each path should not overlap with each other. Therefore, c_1 should satisfy [4]

$$c_1 \geq \max_{1 \leq j \leq J} \frac{2(\alpha_{\text{max}} + k_\nu) + 1}{2N \min_{p,q} (|l_p^j - l_q^j|)}. \quad (29)$$

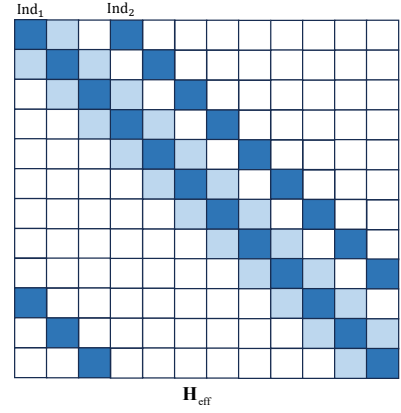


Fig. 5: Illustration of the effective channel matrix of a two-path channel with the system parameters given by $K = 4$, $N = 12$, $l_1 = 0$, $l_2 = 1$, $\nu_1 = 0.05$, $\nu_2 = 0$ and $k_\nu = 1$.

It is shown in [39] that the largest diversity of AFDM can be achieved for c_1 satisfying (29) and c_2 taken as an arbitrary irrational number or a rational number sufficiently smaller than $\frac{1}{2N}$. The above analysis can be readily extended to uplink AFDM-SCMA systems. It is straightforward to show that (29) also holds for the uplink AFDM-SCMA systems, respectively.

Remark 3: It is noted that the proposed AFDM-SCMA can serve as a generic framework and subsumes the existing OFDM-SCMA systems as special cases. Specifically, by setting $c_1 = 0$ and $c_2 = 0$, the IDAFT and DAFT boil down to the IFFT and DFT, respectively, and the proposed AFDM-SCMA system is equivalent to the OFDM-SCMA system.

E. Performance Analysis

In this section, we analyze the performance of the proposed AFDM-SCMA systems. For simplicity, we start with the analysis in the downlink AFDM-SCMA system and then extend the results to uplink channels. Recall (22), it can be rewritten as

$$\mathbf{y}_{\text{sym}} = \sum_{p=1}^P h_p \mathbf{H}_p \mathbf{w}_{\text{sym}} + \mathbf{v}_{\text{sym}} \quad (31)$$

$$= \mathbf{\Phi}(\mathbf{w}_{\text{sym}}) \mathbf{h} + \mathbf{v}_{\text{sym}},$$

where $\mathbf{h} = [h_1, h_2, \dots, h_P]^T \in \mathbb{C}^{P \times 1}$ specifies the channel fading gain of P paths and $\mathbf{\Phi}(\mathbf{w}_{\text{sym}})$ is the $N \times P$ concatenated matrix given by

$$\mathbf{\Phi}(\mathbf{w}_{\text{sym}}) = [\mathbf{H}_1 \mathbf{w}_{\text{sym}} | \dots | \mathbf{H}_P \mathbf{w}_{\text{sym}}]. \quad (32)$$

In (32), each row is a cyclically shifted version of the first row depending on the Doppler tap values. Assume the erroneously decoded codeword is $\hat{\mathbf{w}}_{\text{sym}}$ when \mathbf{w}_{sym} is transmitted, where $\hat{\mathbf{w}}_{\text{sym}} \neq \mathbf{w}_{\text{sym}}$. Then, the PEP between two distinct data matrices $\hat{\mathbf{w}}_{\text{sym}}$ and \mathbf{w}_{sym} is given by

$$\Pr(\hat{\mathbf{w}}_{\text{sym}} \rightarrow \mathbf{w}_{\text{sym}} | \mathbf{h}) = Q \left(\sqrt{\frac{\|\mathbf{\Phi}(\Delta) \mathbf{h}\|^2}{2N_0}} \right), \quad (33)$$

where $\Delta = \hat{\mathbf{w}}_{\text{sym}} - \mathbf{w}_{\text{sym}}$, $\mathbf{\Phi}(\Delta)$ is shown in (30) and δ_i denotes the i th element of Δ . By applying the approximation

$$\Phi(\Delta) = \begin{bmatrix} [H_1]_{1, \text{Ind}_1} \delta_{\text{Ind}_1} & [H_P]_{1, \text{Ind}_P} \delta_{\text{Ind}_P} \\ [H_1]_{1, (1+\text{Ind}_1)_N} \delta_{(1+\text{Ind}_1)_N} & [H_P]_{1, (1+\text{Ind}_P)_N} \delta_{(1+\text{Ind}_P)_N} \\ \vdots & \vdots \\ [H_1]_{1, (N-1+\text{Ind}_1)_N} \delta_{(N-1+\text{Ind}_1)_N} & [H_P]_{1, (N-1+\text{Ind}_P)_N} \delta_{(N-1+\text{Ind}_P)_N} \end{bmatrix}. \quad (30)$$

$Q(x) \approx \frac{1}{12} \exp(-x^2/2) + \frac{1}{4} \exp(-2x^2/3)$ [40], we can rewrite (33) as

$$\Pr(\hat{\mathbf{w}}_{\text{sym}} \rightarrow \mathbf{w}_{\text{sym}} | \mathbf{h}) \approx \frac{1}{12} \exp\left(-\frac{\|\Phi(\Delta) \mathbf{h}\|^2}{4N_0}\right) + \frac{1}{4} \exp\left(-\frac{\|\Phi(\Delta) \mathbf{h}\|^2}{3N_0}\right). \quad (34)$$

Note that $\Phi(\Delta)^H \Phi(\Delta)$ is a Hermitian matrix, its rank and the non-zero eigenvalues are defined as R and $\lambda_i, i = 1, 2, \dots, R$, respectively. Hence, it follows that

$$\begin{aligned} \|\Phi(\Delta) \mathbf{h}\|^2 &= \mathbf{h}^H \Phi(\Delta)^H \Phi(\Delta) \mathbf{h} \\ &= \mathbf{h}^H \mathbf{U} \Sigma \mathbf{U}^H \mathbf{h} \\ &= \tilde{\mathbf{h}}^H \Sigma \tilde{\mathbf{h}}_j \\ &= \sum_{i=1}^R \lambda_i |\tilde{h}_{ji}|^2, \end{aligned} \quad (35)$$

where \mathbf{U} is a unitary matrix, $\tilde{\mathbf{h}} = \mathbf{h}^H \mathbf{U}$ and $\Sigma = \text{diag}\{\lambda_1, \lambda_2, \dots, \lambda_R\}$. Note that $\tilde{\mathbf{h}}$ has the same distribution as \mathbf{h} since it is obtained by multiplying a unitary matrix with \mathbf{h} . We assume each path has independent Rayleigh distribution. Hence, by averaging (17) over the channel statistics, we arrive at

$$\Pr(\hat{\mathbf{w}}_{\text{sym}} \rightarrow \mathbf{w}_{\text{sym}}) \approx \frac{1}{12} \prod_{i=1}^R \frac{1}{1 + \frac{\lambda_i}{4N_0}} + \frac{1}{4} \prod_{i=1}^R \frac{1}{1 + \frac{\lambda_i}{3N_0}}. \quad (36)$$

At high SNRs, i.e., $N_0 \rightarrow 0$, it follows that

$$\Pr(\mathbf{w}_{\text{sym}}^m \rightarrow \mathbf{w}_{\text{sym}}^n) \approx N_0^{-R} \left(\frac{4^R}{12} + \frac{3^R}{4} \right) \prod_{i=1}^R \lambda_i^{-1}. \quad (37)$$

One can see that the rank of $\Phi(\Delta)$ determines the slope of the PEP curve. In general, R is limited by the number of independent fading paths, which is also known as the diversity order [41]. The term $\prod_{i=1}^R \lambda_i$ is also known as the coding gain [41]. The average BER can be formulated as [40]

$$P_e \leq \frac{1}{M^{\frac{JN}{K}} \frac{JN}{K} \log_2 M} \sum_{\mathbf{w}_{\text{sym}}^m} \sum_{\substack{\mathbf{w}_{\text{sym}}^n \\ \mathbf{w}_{\text{sym}}^m \neq \mathbf{w}_{\text{sym}}^n}} \Pr(\mathbf{w}_{\text{sym}}^m \rightarrow \mathbf{w}_{\text{sym}}^n). \quad (38)$$

where $\frac{1}{M^{\frac{JN}{K}} \frac{JN}{K} \log_2 M}$ denotes the probability of each bit in \mathbf{w}_{sym} . In the case of the uplink channels, assume the erroneously decoded codeword is $\hat{\mathbf{x}}_{\text{all}}$ when \mathbf{x}_{all} is transmitted, where $\hat{\mathbf{x}}_{\text{all}} \neq \mathbf{x}_{\text{all}}$. To proceed, we rewrite (24) as

$$\begin{aligned} \mathbf{r}_{\text{sym}} &= \sum_{j=1}^J \Phi(\mathbf{x}_{\text{sym}, j}) \mathbf{h}_j + \mathbf{v}_{\text{sym}} \\ &= \Omega(\mathbf{x}_{\text{all}}) \mathbf{h}_{\text{all}} + \mathbf{v}_{\text{sym}}, \end{aligned} \quad (39)$$

where $\Phi(\mathbf{x}_{\text{sym}, j})$ is the $N \times P_j$ concatenated matrix defined in (32), $\mathbf{h}_{\text{all}} = [\mathbf{h}_1^T, \mathbf{h}_2^T, \dots, \mathbf{h}_J^T]^T$ and $\Omega(\mathbf{x}_{\text{all}}) =$

$[\Phi(\mathbf{x}_{\text{sym}, 1}), \Phi(\mathbf{x}_{\text{sym}, 2}), \dots, \Phi(\mathbf{x}_{\text{sym}, J})]$. We note that the signal model in the uplink channels can be rewritten in the form of (31), hence, the average BER of the uplink AFDM-SCMA systems can be obtained analogue to (31)-(38).

IV. JOINT CODEBOOK AND LOW-COMPLEXITY RECEIVER DESIGN

This section investigates the transceiver design in AFDM-SCMA systems. Specifically, a class of efficient sparse codebooks is first presented to simplify the I/O relation of AFDM-SCMA system. Subsequently, a low-complexity detection and decoding scheme is proposed by utilizing the proposed codebooks.

A. I/O Relation-Inspired Codebook Design

We first introduce the codebook design in downlink AFDM-SCMA systems. Considering the signal model depicted in (21) and (22), it is evident that a two-stage detector is essential at the BS to decode the transmitted codewords. This is due to the difficulties for integrating the codebook superposition process, i.e., (21), and the AFDM transmission process, i.e., (22), into a simplified signal model. In the following, we address this problem through a novel codebook design.

The main steps of the proposed I/O relation-inspired codebook design can be summarized as follows:

Step 1: Let us consider a basic constellation alphabet set \mathcal{A} . By drawing elements from \mathcal{A} , denote its vector form as $\mathbf{a}_0 \in \mathbb{C}^{M \times 1}$.

Step 2: An initial V -dimensional MC, denoted by \mathbf{A}_{MC} , is obtained by a repetition of \mathbf{a}_0 , i.e., $\mathbf{A}_{MC} = [\mathbf{a}_0^T, \mathbf{a}_0^T, \dots, \mathbf{a}_0^T]^T \in \mathbb{C}^{V \times M}$.

Step 3: Phase rotation and power scaling are subsequently applied to each dimension of \mathbf{A}_{MC} to generate multiple codebooks for different users. Specifically, the j th user's codebook is generated by

$$\mathcal{X}_j = \mathbf{V}_j \mathbf{E}_j \Theta_j \mathbf{A}_{MC}, \quad j = 1, 2, \dots, J, \quad (40)$$

where $\mathbf{V}_j \in \mathbb{B}^{K \times V}$ is the codebook mapping matrix that maps a V -dimensional dense constellation to the K -dimensional sparse codebook \mathcal{X}_j , and $\mathbf{E}_j = \text{diag}([\sqrt{E_{j,1}}, \sqrt{E_{j,2}}, \dots, \sqrt{E_{j,V}}]) \in \mathbb{R}^{V \times V}, 0 \leq \forall E_{j,v} \leq V, \sum_{j=1}^J \sum_{v=1}^V E_{j,v} = J$ and $\Theta_j = \text{diag}([e^{i\theta_{j,1}}, e^{i\theta_{j,2}}, \dots, e^{i\theta_{j,V}}]) \in \mathbb{C}^{V \times V}, 0 \leq \forall \theta_{j,v} \leq 2\pi$ are the power scaling and phase rotation matrices of the j th user, respectively. \mathbf{E}_j and Θ_j are designed to scale and rotate \mathbf{A}_{MC} to enhance the constellation shaping gain, thereby improving overall codebook performance. Based on the factor graph, \mathbf{V}_j can be constructed according to the position of the zero elements of \mathbf{f}_j by inserting all-zero row vectors into the

Algorithm 1 I/O Relation-Inspired Codebook Design for AFDM-SCMA Systems

- Require:** $V, \mathbf{F}, \mathbf{Z}_{4 \times 6}$ and $\mathbf{V}_j, j = 1, 2, \dots, J$
- 1: Choose a one-dimensional constellation \mathbf{a}_0 ,
 - 2: Obtain the V -dimensional MC as $\mathbf{A}_{MC} = [\mathbf{a}_0^T, \mathbf{a}_0^T, \dots, \mathbf{a}_0^T]^T \in \mathbb{C}^{V \times M}$,
 - 3: **For uplink channels:**
 - 4: Generate the codebooks as $\mathcal{X}_j = \mathbf{V}_j \mathbf{A}_{MC}, j = 1, 2, \dots, J$,
 - 5: **For downlink channels:**
 - 6: Generate the codebooks as $\mathcal{X}_j = \mathbf{V}_j \mathbf{E}_j \Theta_j \mathbf{A}_{MC}, j = 1, 2, \dots, J$,
 - 7: Optimize \mathbf{Z} to attain large MED.
-

identity matrix \mathbf{I}_V . For example, for the \mathbf{F} given in (2), we have

$$\mathbf{V}_1 = \begin{bmatrix} 0 & 1 & 0 & 0 \\ 0 & 0 & 0 & 1 \end{bmatrix}^T \text{ and } \mathbf{V}_2 = \begin{bmatrix} 1 & 0 & 0 & 0 \\ 0 & 0 & 1 & 0 \end{bmatrix}^T, \quad (41)$$

and $\mathbf{V}_j, j = 3, 4, 5$ and 6 can be generated in a similar way.

Note that the phase rotation matrix and power scaling matrix can be combined together to form a constellation operator matrix, denoted as $\bar{\mathbf{Z}}_j = \mathbf{E}_j \mathbf{R}_j$. We further combine the constellation operation matrix $\bar{\mathbf{Z}}_j$ and mapping matrix \mathbf{V}_j together, i.e., $\mathbf{z}_{K \times 1}^j = \mathbf{V}_j \bar{\mathbf{Z}}_j \mathbf{I}_{K \times 1}$, where \mathbf{I}_K denotes a column vector of K 1's. Hence, the J codebooks can be represented by the signature matrix $\mathbf{Z} = [\mathbf{z}_{K \times 1}^1, \dots, \mathbf{z}_{K \times 1}^J]$. In this paper, the following signature matrix is employed:

$$\mathbf{Z} = \begin{bmatrix} 0 & z_1 & z_2 & 0 & z_3 & 0 \\ z_1 & 0 & z_2 & 0 & 0 & z_3 \\ 0 & z_3 & 0 & z_2 & 0 & z_1 \\ z_3 & 0 & 0 & z_2 & z_1 & 0 \end{bmatrix}, \quad (42)$$

where $z_i = E_i e^{j\theta_i}, 1 \leq i \leq d_f$ and $\sum_{i=1}^{d_f} E_i = d_f/V$. There are d_f distinct rotation angles and power scaling factors at the each dimension of (42) to distinguish the superimposed codewords. With (29) satisfied, each SCMA codeword experiences the same multi-path channel as each path is well separated. Hence, the codebook design criteria becomes the minimum Euclidean distance (MED) of the superimposed constellation [21], [27]. In this paper, E_i and $\theta_i, 1 \leq i \leq d_f$ are optimized to attain large MED. Denote $\Phi_{M^J} = \left\{ \sum_{j=1}^J \mathbf{x}_j \mid \forall \mathbf{x}_j, 0 \leq j \leq J \right\}$ by the superimposed constellation, then the MED of Φ_{M^J} is given by

$$d_{\min}^2 = \min \{ \|\mathbf{w}_n - \mathbf{w}_m\|^2, \forall \mathbf{w}_n, \mathbf{w}_m \in \Phi_{M^J}, \mathbf{w}_n \neq \mathbf{w}_m \}. \quad (43)$$

Specifically, the codebook is optimized with the aid of the Matlab Global Optimization Toolbox.

For uplink channels, to simplify the I/O relation, we employ the low density signature. The phase rotation in **Step 3** is no long required as different users experience different channel conditions [20]. Consequently, the codebook is generated by

$$\mathcal{X}_j = \mathbf{V}_j \mathbf{A}_{MC}, \quad j = 1, 2, \dots, J. \quad (44)$$

The overall codebook design for downlink and uplink AFDM-SCMA is summarized in **Algorithm 1**.

B. Simplified I/O Relation for AFDM-SCMA

Based on the proposed codebooks, we present the simplified I/O relation for the proposed AFDM-SCMA systems. The constellation superposition process in (3) can be re-written as

$$\mathbf{w} = \sum_{j=1}^J \mathbf{x}_j = \mathbf{Z} \mathbf{s}, \quad (45)$$

where $\mathbf{s} = [s_1, s_2, \dots, s_J]^T$, and $s_j \in \mathcal{A}$ denotes transmitted symbol of the j th user. Namely, the input binary message of the j th user are mapped to symbol s_j selected from a constellation alphabet \mathcal{A} . Then the superimposed codeword \mathbf{w} is obtained by multiplying the signature matrix with the input vector \mathbf{s} . The above signal model simplifies the I/O relation of SCMA encoding process whilst maintaining a large MED. Consequently, the signal model of (21) and (22) can be re-written as

$$\begin{aligned} \mathbf{y}_{\text{sym},j} &= \mathbf{H}_{\text{sym},j} \mathbf{Z}_{\text{sym}} \mathbf{s}_{\text{sym}} + \mathbf{z}_{\text{sym},j} \\ &= \bar{\mathbf{H}}_{\text{sym},j} \mathbf{s}_{\text{sym}} + \mathbf{z}_{\text{sym},j}, \end{aligned} \quad (46)$$

where $\mathbf{s}_{\text{sym}} \in \mathbb{C}^{\frac{N}{K} \times 1}$ denotes the input data of $\frac{N}{K}$ SCMA groups, $\mathbf{Z}_{\text{sym}} \in \mathbb{C}^{N \times \frac{N}{K}}$ denotes the effective system signature matrix and $\bar{\mathbf{H}}_{\text{sym},j} = \mathbf{H}_{\text{sym},j} \mathbf{Z}_{\text{sym}} \in \mathbb{C}^{N \times \frac{N}{K}}$ denotes the effective channel matrix for AFDM-SCMA. For localized transmission, \mathbf{Z}_{sym} is a block diagonal matrix, i.e.,

$$\mathbf{Z}_{\text{sym}} = \text{blkdiag} \left\{ \underbrace{\mathbf{Z}, \mathbf{Z}, \dots, \mathbf{Z}}_{N/K} \right\}. \quad (47)$$

Similarly, we can also obtain the effective signature matrix for the interleaved transmission with certain permutation of \mathbf{Z}_{sym} in (47).

Remark 4: Based on the proposed I/O relation-inspired codebook, the SCMA encoding process in (21) and (22) is rewritten in the matrix form with an input dimension of $\frac{N}{K}$. More importantly, the elements in \mathbf{x}_{sym} are independently drawn from the same constellation \mathcal{A} based on the incoming bit messages, and the proposed encoding process can still maintain a large MED.

In uplink SCMA, the encoding process can be rewritten as

$$\mathbf{x}_j = \mathbf{f}_j s_j, \forall s_j \in \mathcal{A}, j = 1, 2, \dots, J, \quad (48)$$

where \mathbf{f}_j is the j th column of \mathbf{F} defined in (2). Hence, similar to the downlink channels, the signal model in (24) can be simplified to

$$\begin{aligned} \mathbf{r}_{\text{sym}} &= \sum_{j=1}^J \mathbf{G}_{\text{sym},j} \mathbf{F}_{\text{sym},j} \mathbf{s}_{\text{sym},j} + \mathbf{v}_{\text{sym}}, \\ &= \bar{\mathbf{G}}_{\text{all}} \mathbf{s}_{\text{all}} + \mathbf{v}_{\text{sym}}, \end{aligned} \quad (49)$$

where $\mathbf{s}_{\text{sym},j} \in \mathbb{C}^{\frac{N}{K} \times 1}$ is the transmitted vector of the j th user in an AFDM symbol, $\mathbf{F}_{\text{sym},j} \in \mathbb{C}^{N \times \frac{N}{K}}$ is the effective system signature matrix, $\bar{\mathbf{G}}_{\text{all}} = [\mathbf{G}_{\text{sym},1} \mathbf{F}_{\text{sym},1}, \mathbf{G}_{\text{sym},2} \mathbf{F}_{\text{sym},2}, \dots, \mathbf{G}_{\text{sym},J} \mathbf{F}_{\text{sym},J}] \in \mathbb{C}^{N \times \frac{N}{K}}$ is the simplified channel matrix of J users, and $\mathbf{s}_{\text{all}} = [\mathbf{s}_{\text{sym},1}^T, \mathbf{s}_{\text{sym},2}^T, \dots, \mathbf{s}_{\text{sym},J}^T]^T \in \mathbb{C}^{\frac{N}{K} \times 1}$ collects input data of J users.

Remark 5: Similar to that of the downlink channels, the input is a length $\frac{N}{K}$ vector, and the elements in \mathbf{s}_{all} are

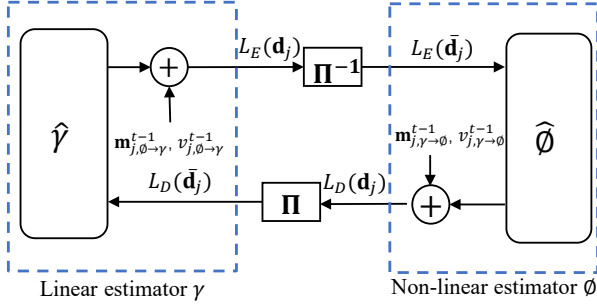


Fig. 6: Illustration of the message propagation of the j th user in the proposed OAMP-assisted iterative receiver.

independently mapped from the input binary messages and drawn from the same alphabet. Compared to the signal model in (24), (49) reduces the dimensions of the channel matrix and input vector from $N \times NJ$ to $N \times \frac{NJ}{K}$ and $NJ \times 1$ to $\frac{NJ}{K} \times 1$, respectively. Such a property allows us to design advanced iterative receiver for the proposed AFDM-SCMA systems.

C. OAMP-assisted Iterative Receiver Design for Coded AFDM-SCMA Systems

By utilizing the proposed I/O relation-inspired codebooks, we are able to simplify the I/O relations of AFDM-SCMA systems, as demonstrated in (46) and (49). The simplified signal models facilitate the application of conventional linear receiver, such as zero forcing and LMMSE, for efficient symbol detection. In this subsection, we introduce an iterative receiver comprising an LMMSE estimator and an LDPC decoder. Note that, the same scheme can be readily extended to downlink channels. The extrinsic information generated by the LMMSE estimator serves as *a priori* information for the user-specific channel decoder, and conversely, the extrinsic information from the channel decoder is used as *a priori* information for the LMMSE estimator.

It is important to note that both (49) and (46) represent overloaded signal models, due to its NOMA transmission nature. To facilitate efficient message passing, new iterative receiver is designed by following the OAMP principles. This approach offers several advantages, including the capability of achieving the LMMSE capacity and the effectiveness in handling ill-conditioned channel matrices and overloaded systems [42]. The key of OAMP is that the linear estimator and the non-linear estimator are designed to be orthogonal in terms of their individual estimation error vectors [42]. The orthogonality of LMMSE and LDPC decoder avoids the estimated errors during the iterative process. As a result, OAMP permits the iterative process gradually converges with stability. For simplicity, denoted $\hat{\gamma}$ and $\hat{\phi}$ by the LMMSE detector and LDPC decoder, respectively. Similarly, denoted γ and ϕ by the corresponding linear and nonlinear estimators, respectively. Fig. 6 shows the message propagation of user j of the proposed OAMP-assisted iterative receiver.

Denote $\mathbf{d}_j = [d_j^1, d_j^2, \dots, d_j^{\log_2(2^M)}]^\mathcal{T}$ by the interleaved bits corresponding to the symbol $s_j \in \mathcal{A}$ of user j with $j = \{1, 2, \dots, J\}$. Note that \mathbf{d}_j is the interleaved coded bits from the channel encoder. We further denote $P(\mathbf{d}_j)$ by the

extrinsic probability generated by the LMMSE detector. To initialize, equiprobable inputs are assumed without *a priori* information from channel decoders. At each iteration, each LMMSE detector outputs $P(\mathbf{d}_j)$ and demaps $P(\mathbf{d}_j)$ to the bit-level log-likelihood ratios (LLRs) as follows:

$$L_E(d_j^m | s_j) \triangleq \ln \frac{\sum_{\forall \mathbf{d}_j: d_j^m=0} P(\mathbf{d}_j)}{\sum_{\forall \mathbf{d}_j: d_j^m=1} P(\mathbf{d}_j)}. \quad (50)$$

The resultant LLRs are further deinterleaved before passing to the channel decoder. Denote $L_E(\bar{\mathbf{d}}_j)$ by the deinterleaved LLRs of the j th user. Upon receiving $L_E(\bar{\mathbf{d}}_j)$, the channel decoder computes an estimation of the information bits and outputs the extrinsic LLRs. The output LLR of the i th deinterleaved bit is expressed as [42]–[44]

$$L_D(\bar{\mathbf{d}}_j[i]) \triangleq \log \frac{\Pr(\bar{\mathbf{d}}_j[i] = 0 | L_E(\bar{\mathbf{d}}_j))}{\Pr(\bar{\mathbf{d}}_j[i] = 1 | L_E(\bar{\mathbf{d}}_j))}, \quad (51)$$

where $L_D(\bar{\mathbf{d}}_j)$ is the extrinsic LLR of the channel decoder output. Similarly, the extrinsic LLRs are interleaved as $L_D(\mathbf{d}_j)$ and utilized as the input *a priori* information of the LMMSE detector.

1) Messaging passing from LMMSE to channel decoder:

Following the LMMSE estimation principles, the *a posteriori* mean and covariance matrix at the t th iteration can be estimated as [45]

$$\begin{aligned} \mathbf{V}_{\text{det}}^t &= \left(\bar{\mathbf{G}}_{\text{all}} (\mathbf{V}_{\phi \rightarrow \gamma}^{t-1})^{-1} \bar{\mathbf{G}}_{\text{all}} + (\mathbf{V}_{\phi \rightarrow \gamma}^{t-1})^{-1} \right)^{-1}, \\ \mathbf{m}_{\text{det}}^t &= \mathbf{V}_{\text{det}}^t \left(\bar{\mathbf{G}}_{\text{all}}^\mathcal{T} (\mathbf{V}_{\phi \rightarrow \gamma}^{t-1})^{-1} \mathbf{r}_{\text{sym}} + (\mathbf{V}_{\phi \rightarrow \gamma}^{t-1})^{-1} \mathbf{m}_{\phi \rightarrow \gamma}^{t-1} \right), \end{aligned} \quad (52)$$

where $\mathbf{V}_{\phi \rightarrow \gamma}^{t-1} = \text{diag}([\mathbf{v}_1^{1,t-1}, \mathbf{v}_2^{2,t-1}, \dots, \mathbf{v}_j^{Q,t-1}])$ and $\mathbf{m}_{\phi \rightarrow \gamma}^{t-1} = [\mathbf{m}_{\phi \rightarrow \gamma}^{1,t-1}, \mathbf{m}_{\phi \rightarrow \gamma}^{2,t-1}, \dots, \mathbf{m}_{\phi \rightarrow \gamma}^{Q,t-1}]$ are the variance and mean matrices from the LDPC decoder to the LMMSE detector at the t -1th iteration, respectively, and $\mathbf{m}_{\phi \rightarrow \gamma}^{q,t-1} = [m_1^{q,t-1}, m_2^{q,t-1}, \dots, m_j^{q,t-1}]$ and $\mathbf{v}^{q,t-1} = [v_1^{q,t-1}, v_2^{q,t-1}, \dots, v_j^{q,t-1}]$ are the corresponding mean and variance vectors at the q th block of user j . For the overloaded signal model, we utilize the matrix inverse lemma to reduce the computational complexity of (52). Specifically, (52) can be rewritten as

$$\begin{aligned} \mathbf{V}_{\text{det}}^t &= \mathbf{V}_{\phi \rightarrow \gamma}^{t-1} - \mathbf{W}_{\text{MMSE}}^t \bar{\mathbf{G}}_{\text{all}} \mathbf{V}_{\phi \rightarrow \gamma}^{t-1}, \\ \mathbf{m}_{\text{det}}^t &= \mathbf{m}_{\phi \rightarrow \gamma}^{t-1} + \mathbf{W}_{\text{MMSE}}^t (\mathbf{r}_{\text{sym}} - \bar{\mathbf{G}}_{\text{all}} \mathbf{m}_{\phi \rightarrow \gamma}^{t-1}), \end{aligned} \quad (53)$$

where

$$\mathbf{W}_{\text{MMSE}}^t = \mathbf{V}_{\phi \rightarrow \gamma}^{t-1} \bar{\mathbf{G}}_{\text{all}}^\mathcal{T} \left(\mathbf{V}_{\phi \rightarrow \gamma}^{t-1} + \bar{\mathbf{G}}_{\text{all}} \mathbf{V}_{\phi \rightarrow \gamma}^{t-1} \bar{\mathbf{G}}_{\text{all}}^\mathcal{T} \right)^{-1}. \quad (54)$$

Let $\mathbf{v}_{j,\text{det}}^t = [v_{j,\text{det}}^{1,t}, v_{j,\text{det}}^{2,t}, \dots, v_{j,\text{det}}^{Q,t}]^\mathcal{T}$, $\forall v_{j,\text{det}}^{q,t} \in \mathbf{V}_{\text{det}}^t$ and $\mathbf{v}_{j,\phi \rightarrow \gamma}^{t-1} = [v_{j,\phi \rightarrow \gamma}^{1,t-1}, v_{j,\phi \rightarrow \gamma}^{2,t-1}, \dots, v_{j,\phi \rightarrow \gamma}^{Q,t-1}]^\mathcal{T}$, $\forall v_{j,\phi \rightarrow \gamma}^{q,t-1} \in \mathbf{V}_{\phi \rightarrow \gamma}^{t-1}$ be the variance vectors of the j th user at the t th and $(t-1)$ -th iterations. Let us define

$$\begin{aligned} \bar{v}_{j,\text{det}}^t &= \frac{1}{Q} \|\mathbf{v}_{j,\text{det}}^t\|^2, \\ \bar{v}_{j,\phi \rightarrow \gamma}^{t-1} &= \frac{1}{Q} \|\mathbf{v}_{j,\phi \rightarrow \gamma}^{t-1}\|. \end{aligned} \quad (55)$$

Following the message combining rule in OAMP [42], we update the mean and variance from the LMMSE to the LDPC decoder as

$$\begin{aligned} v_{j,\gamma \rightarrow \phi}^t &= \left(\frac{1}{\bar{v}_{j,\text{det}}^t} - \frac{1}{\bar{v}_{j,\phi \rightarrow \gamma}^{t-1}} \right)^{-1}, \\ \mathbf{m}_{j,\gamma \rightarrow \phi}^t &= v_{j,\gamma \rightarrow \phi}^t \left(\frac{\mathbf{m}_{j,\text{det}}^t}{\bar{v}_{j,\text{det}}^t} - \frac{\mathbf{m}_{j,\phi \rightarrow \gamma}^{t-1}}{\bar{v}_{j,\phi \rightarrow \gamma}^{t-1}} \right). \end{aligned} \quad (56)$$

To enhance algorithmic performance and regulate the convergence speed, we employ a damping factor $\kappa \in (0, 1]$ and update the mean and variance as [46]

$$\begin{aligned} v_{j,\gamma \rightarrow \phi}^t &= \left(\frac{\kappa}{\bar{v}_{j,\text{det}}^t} - \frac{1-\kappa}{\bar{v}_{j,\phi \rightarrow \gamma}^{t-1}} \right)^{-1}, \\ \mathbf{m}_{j,\gamma \rightarrow \phi}^t &= v_{j,\gamma \rightarrow \phi}^t \left(\kappa \frac{\mathbf{m}_{j,\text{det}}^t}{\bar{v}_{j,\text{det}}^t} - (1-\kappa) \frac{\mathbf{m}_{j,\phi \rightarrow \gamma}^{t-1}}{\bar{v}_{j,\phi \rightarrow \gamma}^{t-1}} \right). \end{aligned} \quad (57)$$

Denote s_j^c by the c th symbol in an LDPC block, then based on the updated mean and variance, the *a posteriori* probability of s_j^c can be decomposed as follows

$$P(s_j^c = \mathcal{C}) \propto \exp \left(- \frac{|\mathcal{C} - m_{j,\gamma \rightarrow \phi}^{c,t}|^2}{v_{j,\gamma \rightarrow \phi}^t} \right), \forall \mathcal{C} \in \mathcal{A}. \quad (58)$$

By (50), the extrinsic LLRs of the LMMSE can be obtained. For QPSK constellation, the LLR can be computed efficiently as [45]

$$\begin{aligned} L_E(d_j^{c,1} | s_j^c) &= \frac{\sqrt{8} \text{Re}\{m_{j,\gamma \rightarrow \phi}^{c,t}\}}{v_{j,\gamma \rightarrow \phi}^t}, \\ L_E(d_j^{c,2} | s_j^c) &= \frac{\sqrt{8} \text{Im}\{m_{j,\gamma \rightarrow \phi}^{c,t}\}}{v_{j,\gamma \rightarrow \phi}^t}. \end{aligned} \quad (59)$$

2) Message passing from channel decoder to LMMSE:

As mentioned, the extrinsic LLR of LMMSE estimator is deinterleaved before passing to the channel decoder. After channel decoding, the LDPC decoder outputs new extrinsic information $L_D(\bar{\mathbf{d}}_j)$, defined in (51). Through interleaver, $L_D(\mathbf{d}_j)$ is obtained. Upon obtaining the extrinsic LLRs from the channel decoder, $L_D(\mathbf{d}_j)$ is mapped to *a priori* probabilities, i.e.,

$$\begin{aligned} P_D(s_j^c = \mathcal{C}) &= \prod_{i=1}^{\log_2(M)} \frac{\exp(-\Psi_{\mathcal{C}}[i] L_D(\mathbf{d}_j[c \log_2(M) + i]))}{1 + \exp(L_D(\mathbf{d}_j[c \log_2(M) + i]))} \\ &\propto \prod_{i=1}^{\log_2(M)} \exp(-\Psi_{\mathcal{C}}[i] L_D(\mathbf{d}_j[c \log_2(M) + i])), \end{aligned} \quad (60)$$

where $\Psi_{\mathcal{C}}[i] \in \{0, 1\}$ denotes the labeling value of the i th bit of \mathcal{C} . The prior probabilities $P_D(s_j)$ are then projected into Gaussian distribution with its mean and variance respectively given by

$$\begin{aligned} m_{j,\text{dec}}^{c,t} &\triangleq \sum_{\mathcal{C} \in \mathcal{S}} \mathcal{C} P(s_j^c = \mathcal{C}), \\ v_{j,\text{dec}}^{c,t} &\triangleq \sum_{\mathcal{C} \in \mathcal{S}} |\mathcal{C}|^2 P_D(s_j^c = \mathcal{C}) - |m_{j,\text{dec}}^{c,t}|^2. \end{aligned} \quad (61)$$

For QPSK constellation, the mean and variance can be computed efficiently by as in [45]

$$\begin{aligned} m_{j,\text{dec}}^{c,t} &= \frac{\sqrt{2}}{2} \left(\tanh(L_D(\mathbf{d}_j[c \log_2(M) + 1])) + \right. \\ &\quad \left. i \tanh \left(L_D \left(\frac{\mathbf{d}_j[c \log_2(M) + 2]}{2} \right) \right) \right), \\ v_{j,\text{dec}}^{c,t} &= 1 - |m_{j,\text{dec}}^c|^2, \end{aligned} \quad (62)$$

respectively. Let $\mathbf{m}_{j,\text{dec}}^t$ and $\mathbf{v}_{j,\text{dec}}^t$ denote the mean and variance vectors for each LDPC frame with its c th entry given by $m_{j,\text{dec}}^{c,t}$ and $v_{j,\text{dec}}^{c,t}$, respectively. Define

$$\bar{v}_{j,\text{dec}}^t = \frac{1}{B} \|\mathbf{v}_{j,\text{dec}}^t\|^2, \quad (63)$$

where B is length of $\mathbf{v}_{j,\text{dec}}^t$, i.e. the number of symbols within an LDPC frame. Then, the mean and variance are updated respectively as

$$\begin{aligned} v_{j,\phi \rightarrow \gamma}^t &= \left(\frac{\kappa}{\bar{v}_{j,\text{dec}}^t} - \frac{1-\kappa}{v_{j,\gamma \rightarrow \phi}^{t-1}} \right)^{-1}, \\ \mathbf{m}_{j,\phi \rightarrow \gamma}^t &= v_{j,\phi \rightarrow \gamma}^t \left(\kappa \frac{\mathbf{m}_{j,\text{dec}}^t}{\bar{v}_{j,\text{dec}}^t} - (1-\kappa) \frac{\mathbf{m}_{j,\gamma \rightarrow \phi}^{t-1}}{v_{j,\gamma \rightarrow \phi}^{t-1}} \right). \end{aligned} \quad (64)$$

Finally, the new means and variances will feed back to the LMMSE estimator and utilized as *a priori* information.

D. State Evolution

State evolution (SE) is a recursive procedure that tracks the mean square error (MSE) of local estimators during iterative processing. In this subsection, we briefly present the SE in the proposed OAMP-assisted receiver design. The readers are referred to [42]–[44], [47] for more details about the SE derivation in OAMP. To proceed, in what follows, we assume that the input and output errors of LE and NLE are independent of each other. Let τ^t and η^t by the MSEs of $\mathbf{m}_{\gamma \rightarrow \phi}^t$ and $\mathbf{m}_{\phi \rightarrow \gamma}^t$, respectively. Namely,

$$\tau_t = \frac{NJ}{K} \mathbb{E} [\|\mathbf{m}_{\gamma \rightarrow \phi}^t - \mathbf{s}\|^2], \eta_t = \frac{NJ}{K} \mathbb{E} [\|\mathbf{m}_{\phi \rightarrow \gamma}^t - \mathbf{s}\|^2]. \quad (65)$$

Then, SE refers to the following recursions of τ_t and η_t :

$$\begin{aligned} \tau_t &= \gamma_{\text{SE}}(\eta_t) = \left([\hat{\gamma}_{\text{SE}}(\eta_t)]^{-1} - \eta_t^{-1} \right)^{-1}, \\ \eta_{t+1} &= \phi_{\text{SE}}(\tau_t) = \left([\hat{\phi}_{\text{SE}}(\tau_t)]^{-1} - \tau_t^{-1} \right)^{-1}, \end{aligned} \quad (66)$$

where

$$\begin{aligned} \hat{\gamma}_{\text{SE}}(\eta) &= \text{mmse}\{\mathbf{s} | \sqrt{\eta} \mathbf{s} + \mathbf{z}_s, \gamma\}, \\ &= \eta - \frac{NJ}{K} \eta^2 \text{Tr} \left(\bar{\mathbf{G}}_{\text{all}}^H \left(\eta \bar{\mathbf{G}}_{\text{all}} \bar{\mathbf{G}}_{\text{all}}^H + N_0 \mathbf{I} \right)^{-1} \bar{\mathbf{G}}_{\text{all}} \right), \\ \hat{\phi}_{\text{SE}}(\tau) &= \frac{1}{J} \sum_{j=1}^J \text{mmse}\{\mathbf{s}_j | \mathbf{s}_j + \sqrt{\tau} \mathbf{z}_s, \phi\}, \end{aligned} \quad (67)$$

where $\mathbf{z}_s \in \mathcal{N}(\mathbf{0}, \mathbf{I})$, \mathbf{s}_j is the modulated symbol for the j th NLE and $\text{mmse}\{a|b\} = \mathbb{E} \{(a - \mathbb{E}(a|b))^2\}$. Unfortunately, it is quite difficult, if not impossible, to obtain a close-form of $\text{mmse}\{\mathbf{s}_j | \mathbf{s}_j + \sqrt{\tau} \mathbf{z}_s, \phi\}$ for an NLE with LDPC codes. Here, Monte Carlo simulation is employed to obtain the MSE of NLE outputs.

TABLE I: Simulation Parameters

Parameters	Values
SCMA setting	$\xi = 150\%$, $K = 4$, $J = 6$
SCMA codewords allocation	Localized and interleaved
Codebooks	The proposed codebook and Chen's codebook [20]
Channel model	EVA channel [48]
Number of AFDM SCs	$N = 128$
CPP length	24
Carrier frequency	4 GHz
SC spacing	15 KHz
User speed	300 Km/h
Maximum Doppler shift (ν_{\max})	1.1 KHz

V. NUMERICAL RESULTS

In this section, we present numerical simulation results to validate the performance of the proposed AFDM-SCMA systems. The SCMA system with the indicator matrix given in (2) is employed. The QPSK constellation is employed as the basic constellation, i.e., $\mathcal{A} = \{0.707 + 0.707i, 0.707 - 0.707i, -0.707 + 0.707i, -0.707 - 0.707i\}$, for generating the I/O codebooks and the resultant signature matrices for uplink and downlink channels are respectively given as $\mathbf{Z}_{\text{UL}} = \mathbf{F}_{4 \times 6}$ and

$$\mathbf{Z}_{\text{DL}} = \begin{bmatrix} 0 & 1.07i & 0.53 & 0 & 0.27 & 0 \\ 1.07i & 0 & 0.53 & 0 & 0 & 0.27 \\ 0 & 0.27 & 0 & 0.53 & 0 & 1.07i \\ 0.27 & 0 & 0 & 0.53 & 1.07i & 0 \end{bmatrix}. \quad (68)$$

A. Computational Complexity

Since the same channel codes are employed for both the proposed OAMP-assisted receiver and the conventional turbo receiver, we focus on comparing the computational complexities of the multi-user detection modules. The computational complexity of the LMMSE estimator is dominated by the matrix inverse in (53), which can be approximated as $\mathcal{O}(N^3)$. The computational complexity of MPA for each SCMA group is given by $\mathcal{O}(I_t K M^{d_f} d_f)$, where I_t denotes the number of MPA iterations. Hence, the computational complexity of MPA for an AFDM-SCMA symbol is given by $\mathcal{O}(I_t N M^{d_f} d_f)$. In the proposed OAMP-assisted receiver, the MPA is no longer required, resulting in a complexity reduction ratio (CRR) approximated by

$$\text{CRR} = 1 - \frac{N^3}{I_t N M^{d_f} d_f + N^3}. \quad (69)$$

For a system setting with $N = 64$, $d_f = 3$, $I_t = 6$ and $M = 4$, the CRR is given by $\text{CRR} = 78\%$.

B. Uncoded BER Performance

We first present the simulated and analytical BER performance of the proposed AFDM-SCMA in uplink channels with a generalized MPA detector presented in Section III-C. Specifically, we consider $J = 6$ users communicate over $N = 8$ AFDM SCs, and choose the binary phase-shift keying (BPSK) as the basic alphabet \mathcal{A} . Fig. 7 shows the BER performance of the proposed AFDM-SCMA and the conventional OFDM-SCMA systems over a two-path and

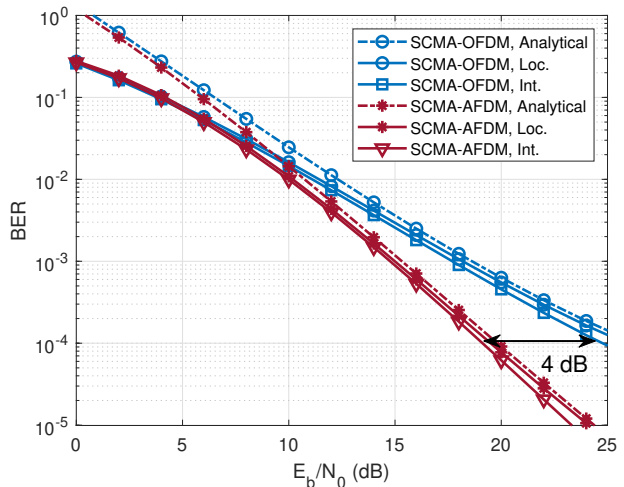
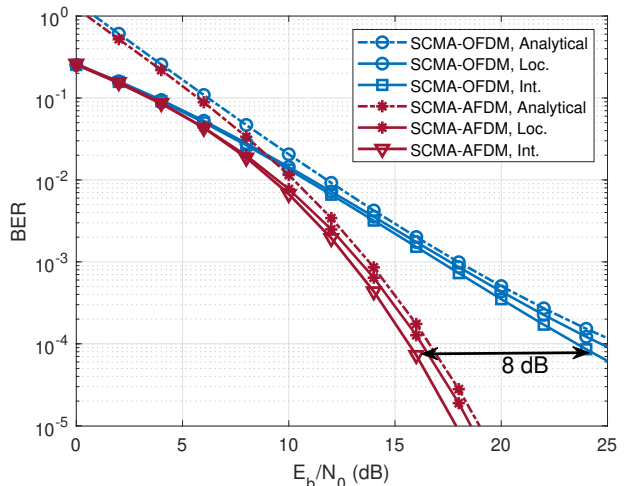
(a) $P = 2$ (b) $P = 3$

Fig. 7: Simulated and analytical BER comparisons of the proposed AFDM-SCMA and OFDM-SCMA systems in uplink channels.

three-path fading channels, where each path is assumed to be independent and identically distributed with its variance given by $1/P$. The curves with “Int.” and “Loc.” denote the interleaved and localized transmissions, respectively. “CB” denotes the abbreviation of codebook. Notably, all the simulated BERs match well with the theoretical analysis at medium-to-high SNR values. At low SNRs, a discrepancy between the analytical and simulated BER is observed. This is due to the fact that the approximation in (34) is more accurate at high SNRs. In addition, the proposed AFDM-SCMA outperforms conventional OFDM-SCMA significantly. Specifically, about 8 dB E_b/N_0 gain is observed for the proposed AFDM-SCMA.

We now evaluate the performance of the proposed AFDM-SCMA in downlink channels with the two-stage detector presented in Section III-B. The MPA iteration number is 5, and codebooks developed in (68) are employed. Refer to Table I for detailed simulation parameters. The EVA channel model is considered, where the

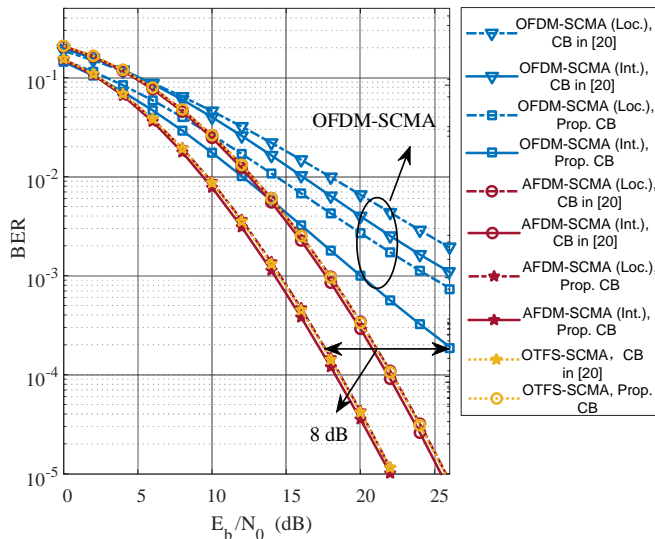


Fig. 8: BER performance comparison of AFDM-SCMA, OTFS-SCMA and OFDM-SCMA in downlink channels.

power delay profile is given by $[0, -1.5, -1.4, -3.6, -0.6, -9.1, -7.0, -12.0, -16.9]$ dB against the excess tap delays $[0, 30, 150, 310, 370, 710, 1090, 1730, 2510]$ ns [48]. The Doppler shift at the p th path of the j th user is given by $\nu_{p,j} = \nu_{\max} \cos(\psi_{p,i})$ where $\psi_{p,i}$ has a uniform distribution $\psi_{p,i} \sim \mathcal{U}[-\pi, \pi]$. The OTFS-SCMA scheme proposed in [28] is also employed for comparison. Specifically, we consider the interleaved scheme with the total numbers of the delay and the Doppler bins given by 8 and 16, respectively. As seen from Fig. 8, the BER performance of OFDM-SCMA systems deteriorates for the localized transmission scheme compared to that of the interleaved schemes due to the potential deep fades within several consecutive SCs. However, the AFDM-SCMA with interleaved and localized transmissions achieve similar BER performances. This is due to 1) the intrinsic time-frequency spreading gain by AFDM transmission; 2) the chirp-rate tuning which leads to well separated multipath channels separated in the effective channel matrix. The proposed codebook achieves about 4 dB gain over Chen's codebook [20] at the $\text{BER} = 10^{-4}$ for the proposed AFDM-SCMA system. In addition, the proposed AFDM-SCMA achieves a BER performance very close to that of the OTFS-SCMA scheme as both can achieve the full channel diversity. However, as mentioned earlier, the proposed AFDM-SCMA enjoys the benefits of lower implementation complexity and channel estimation overhead compared to OTFS-SCMA [4], [8]. In the next subsection, we will show that the proposed I/O codebook and low-complexity receiver can also be utilized for OTFS-SCMA systems. Moreover, the proposed AFDM-SCMA outperforms the OFDM-SCMA system significantly. In particular, 8 dB gain is observed with the proposed codebook at the $\text{BER} = 2 \times 10^{-4}$. Again, it is emphasized that the OFDM-SCMA system is the special case of the proposed systems with $c_1 = 0$ and $c_2 = 0$.

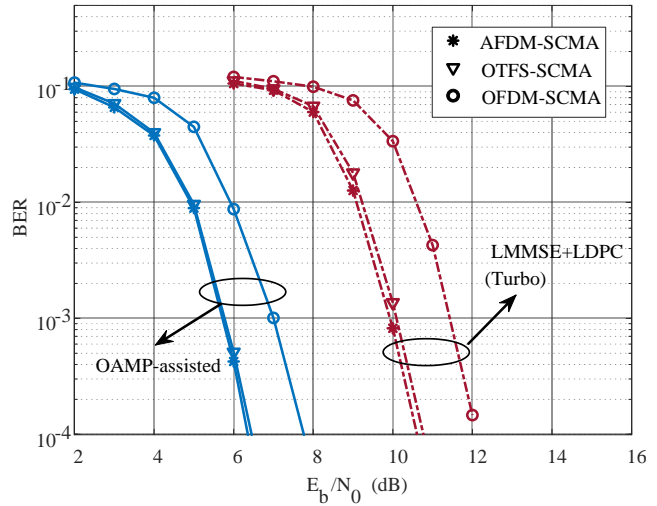


Fig. 9: Coded BER comparison of AFDM-SCMA, OTFS-SCMA and OFDM-SCMA in downlink channels.

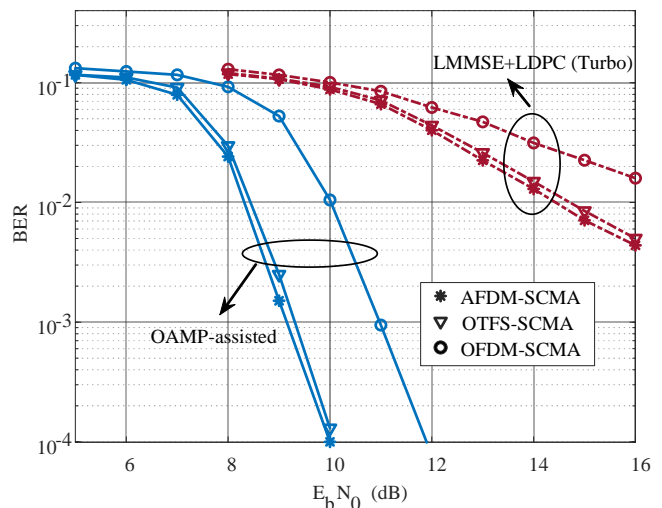


Fig. 10: Coded BER comparison of AFDM-SCMA, OTFS-SCMA and OFDM-SCMA in uplink channels.

C. Coded BER Performance

This subsection evaluates the BER performances of the LDPC-coded AFDM-SCMA systems over EVA channels. The interleaved transmissions for AFDM-SCMA, OTFS-SCMA and OFDM-SCMA are considered. The 5G NR LDPC code, as specified in TS38.212 [49], with frame length of 2048 and rate of $2/3$ is considered. Table I presents the detailed channel model and system parameters. The inner LDPC iteration and outer OAMP iteration numbers are set to be 8 and 10, respectively. In addition, the damping factor is set as $\kappa = 0.25$. We also implement the conventional turbo receiver as the benchmark scheme. The turbo decoding is carried out between LMMSE and channel decoder by iteratively exchanging soft information in the form of LLR including *a priori* LLR and *a posteriori* LLR (extrinsic) [40]. For fair comparison, the number of iterations in the turbo receiver equals that of the proposed receiver.

Fig. 9 shows the coded BER performance of the proposed OAMP-enhanced receiver with the proposed I/O inspired-

VI. CONCLUSION

In this paper, we have proposed an AFDM empowered SCMA system, referred to as AFDM-SCMA, for massive connectivity in high mobility channels. The signal model, multi-user detection, system parameters and the BER performance of the proposed AFDM-SCMA have been discussed in details. A class of I/O-inspired codebook has been proposed, which allows the receiver to utilize the ZF and LMMSE detectors. Building upon these codebooks, we have introduced an OAMP assisted iterative detection and decoding scheme for both downlink and uplink channels. Our numerical results have shown that the proposed AFDM-SCMA significantly outperforms OFDM-SCMA in both uncoded and coded systems. The simulation results have demonstrated that the proposed receiver can significantly enhance the BER performance while reducing the decoding complexity. Moreover, we have also shown that the proposed receiver can be utilized in OTFS-SCMA for low-complexity detection.

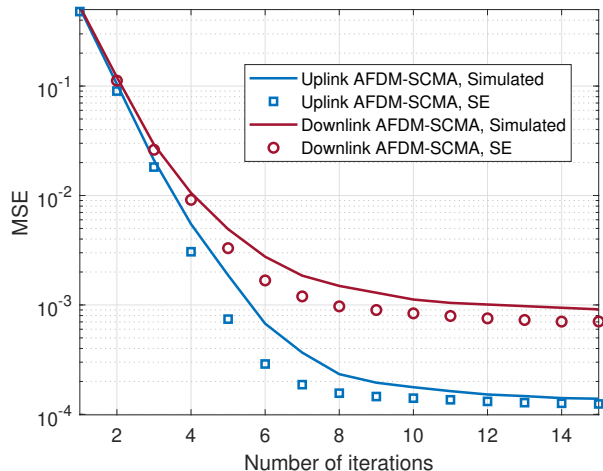


Fig. 11: MSE performance v.s. Number of iterations

codebook over downlink channels. The two-stage detector proposed in [28] is also implemented for comparison. The main observations are summarized as follows:

- Our proposed joint codebook and receiver design notably enhance BER performance. Since MPA is not required, hence the proposed receiver significantly reduces the detection complexity.
- The proposed receiver significantly outperforms the turbo receiver significantly. For overloaded multiuser systems, the error performance of turbo receiver may degrade significantly since it cannot guarantee the orthogonality between the input and the output errors.
- The proposed AFDM-SCMA in conjunction with the proposed receiver achieves about 1.5 dB gain over the OFDM-SCMA systems in EVA channels.
- Our proposed I/O codebook and OAMP-assisted receiver can be also employed in OTFS-SCMA for performance enhancement and low-complexity detection. Notably, the OTFS-SCMA with the proposed codebook and receiver achieves a similar BER performance with that of the proposed AFDM-SCMA and significantly outperforms OFDM-SCMA.

Fig. 10 compares the coded BER performances of the proposed AFDM-SCMA and OFDM-SCMA in uplink channels. The advantage of AFDM-SCMA is more prominent in the uplink channels, with a noticeable gain of about 2 dB using the proposed receiver. Similar to the case of the downlink channels, the BER performance of the turbo receiver deteriorates significantly.

Fig. 11 depicts the MSE behaviors with the number of iterations of the proposed receiver in both downlink and uplink channels, where the E_b/N_0 values are fixed to be 5 dB and 9 dB, respectively. It is evident that the simulated MSEs match well with the predicted MSEs by SE, demonstrating the effectiveness of SE for analyzing the convergence that the performance of the proposed receiver.

REFERENCES

- [1] M. Noor-A-Rahim, Z. Liu, H. Lee, M. O. Khyam, J. He, D. Pesch, K. Moessner, W. Saad, and H. V. Poor, "6G for vehicle-to-everything (V2X) communications: Enabling technologies, challenges, and opportunities," *Proc. IEEE*, vol. 110, no. 6, pp. 712–734, June 2022.
- [2] Y. Zhou, H. Yin, J. Xiong, S. Song, J. Zhu, J. Du, H. Chen, and Y. Tang, "Overview and performance analysis of various waveforms in high mobility scenarios," Feb. 2023. [Online]. Available: <https://arxiv.org/abs/2302.14224>
- [3] T. Wang, J. Proakis, E. Masry, and J. Zeidler, "Performance degradation of OFDM systems due to Doppler spreading," *IEEE Trans. Wireless Commun.*, vol. 5, no. 6, pp. 1422–1432, June 2006.
- [4] A. Bemani, N. Ksairi, and M. Kountouris, "Affine frequency division multiplexing for next generation wireless communications," *IEEE Trans. Wireless Commun.*, pp. 8214–8229, Nov. 2023.
- [5] T. Erseghe, N. Laurenti, and V. Cellini, "A multicarrier architecture based upon the affine Fourier transform," *IEEE Trans. Commun.*, vol. 53, no. 5, pp. 853–862, May 2005.
- [6] S.-C. Pei and J.-J. Ding, "Closed-form discrete fractional and affine Fourier transforms," *IEEE Trans. Signal Process.*, vol. 48, no. 5, pp. 1338–1353, May 2000.
- [7] X. Ouyang and J. Zhao, "Orthogonal chirp division multiplexing," *IEEE Trans. Commun.*, vol. 64, no. 9, pp. 3946–3957, Sept. 2016.
- [8] H. Yin, X. Wei, Y. Tang, and K. Yang, "Diagonally reconstructed channel estimation for MIMO-AFDM with inter-doppler interference in doubly selective channels," Jun. 2022. [Online]. Available: <https://arxiv.org/abs/2206.12822>
- [9] Q. Wang, A. Kakkavas, X. Gong, and R. A. Stirling-Gallacher, "Towards integrated sensing and communications for 6G," in *2nd IEEEJC&S*. IEEE, 2022, pp. 1–6.
- [10] Y. Ni, Z. Wang, P. Yuan, and Q. Huang, "An AFDM-based integrated sensing and communications," in *ISWCS*, Hangzhou, China, 2022, pp. 1–6.
- [11] Y. Liu, S. Zhang, X. Mu, Z. Ding, R. Schober, N. Al-Dhahir, E. Hossain, and X. Shen, "Evolution of NOMA toward next generation multiple access (NGMA) for 6G," *IEEE J. Sel. Areas Commun.*, vol. 40, no. 4, pp. 1037–1071, April 2022.
- [12] Q. Luo, P. Gao, Z. Liu, L. Xiao, Z. Mheich, P. Xiao, and A. Maaref, "An error rate comparison of power domain non-orthogonal multiple access and sparse code multiple access," *IEEE Open J. Commun. Society*, vol. 2, pp. 500–511, Sept. 2021.
- [13] Q. Luo, Z. Mheich, G. Chen, P. Xiao, and Z. Liu, "Reinforcement learning aided link adaptation for downlink NOMA systems with channel imperfections," in *2023 IEEE WCNC*, Glasgow, United Kingdom, Sept. 2023, pp. 1–6.
- [14] W. Yuan, N. Wu, Q. Guo, Y. Li, C. Xing, and J. Kuang, "Iterative receivers for downlink MIMO-SCMA: Message passing and distributed cooperative detection," *IEEE Trans. Wireless Commun.*, vol. 17, no. 5, pp. 3444–3458, May 2018.

- [15] T. Lei, S. Ni, N. Cheng, S. Chen, and X. Song, "SCMA codebook for uplink rician fading channels," *IEEE Commun Lett.*, vol. 27, no. 2, pp. 527–531, Feb. 2022.
- [16] H. Wen *et al.*, "Designing enhanced multidimensional constellations for code-domain NOMA," *IEEE wireless commun. lett.*, vol. 11, no. 10, pp. 2130–2134, Oct. 2022.
- [17] Q. Luo, Z. Liu, G. Chen, P. Xiao, Y. Ma, and A. Maaref, "A design of low-projection SCMA codebooks for ultra-low decoding complexity in downlink iot networks," *IEEE Trans. Wireless Commun.*, vol. 22, no. 10, pp. 6608–6623, Oct. 2023.
- [18] Y.-M. Chen, P.-H. Wang, C.-S. Cheng, and Y.-L. Ueng, "A joint design of SCMA codebook and PTS-based PAPR reduction for downlink OFDM scheme," *IEEE Trans. Vehi. Technol.*, vol. 71, no. 11, pp. 11 936–11 948, Nov. 2022.
- [19] T. Lei *et al.*, "A progressive codebook optimization scheme for sparse code multiple access in downlink channels." [Online]. Available: <https://arxiv.org/abs/2403.16826>
- [20] Y.-M. Chen and J.-W. Chen, "On the design of near-optimal sparse code multiple access codebooks," *IEEE trans. commun.*, vol. 68, no. 5, pp. 2950–2962, May 2020.
- [21] Q. Luo, Z. Liu, G. Chen, Y. Ma, and P. Xiao, "A novel multitask learning empowered codebook design for downlink SCMA networks," *IEEE Wireless Commun. Lett.*, vol. 11, no. 6, pp. 1268–1272, June 2022.
- [22] X. Li, Z. Gao, Y. Gui, Z. Liu, P. Xiao, and L. Yu, "Design of power-imbalanced SCMA codebook," *IEEE Trans. Vehi. Techno.*, vol. 71, no. 2, pp. 2140–2145, Feb. 2022.
- [23] Y. Zheng *et al.*, "A low-complexity codebook design scheme for SCMA systems over an AWGN channel," *IEEE Trans. Vehi. Techno.*, vol. 71, no. 8, pp. 8675–8688, Aug. 2022.
- [24] L. Chai, Z. Liu, P. Xiao, A. Maaref, and L. Bai, "An improved EPA-based receiver design for uplink LDPC coded SCMA system," *IEEE Wireless Commun. Lett.*, vol. 11, no. 5, pp. 947–951, May 2022.
- [25] W. Yuan, N. Wu, Q. Guo, Y. Li, C. Xing, and J. Kuang, "Iterative receivers for downlink MIMO-SCMA: Message passing and distributed cooperative detection," *IEEE Trans. Wireless Commun.*, vol. 17, no. 5, pp. 3444–3458, May 2018.
- [26] Y. Ge, Q. Deng, D. G. G., Y. L. Guan, and Z. Ding, "OTFS signaling for SCMA with coordinated multi-point vehicle communications," *IEEE Trans. on Veh. Technol.*, vol. 72, no. 7, pp. 9044–9057, July 2023.
- [27] H. Wen, W. Yuan, Z. Liu, and S. Li, "OTFS-SCMA: A downlink NOMA scheme for massive connectivity in high mobility channels," *IEEE Trans. Wireless Commun.*, pp. 5770–5784, Sept. 2023.
- [28] K. Deka, A. Thomas, and S. Sharma, "OTFS-SCMA: A code-domain NOMA approach for orthogonal time frequency space modulation," *IEEE Trans. Commun.*, vol. 69, no. 8, pp. 5043–5058, May 2021.
- [29] Y. Ge, L. Liu, S. Huang, D. González, Y. L. Guan, and Z. Ding, "Low-complexity memory amp detector for high-mobility MIMO-OTFS SCMA systems," in *2023 IEEE ICC Workshops*. Rome, Italy: IEEE, 2023, pp. 807–812.
- [30] Q. Deng, Y. Ge, and Z. Ding, "Jamming suppression via resource hopping in high-mobility OTFS-SCMA systems," *IEEE Wireless Commun. Lett.*, vol. 12, no. 12, pp. 2138–2142, Dec. 2023.
- [31] W. Yuan, Z. Wei, J. Yuan, and D. W. K. Ng, "A simple variational bayes detector for orthogonal time frequency space (OTFS) modulation," *IEEE Trans. Vehi. Technol.*, vol. 69, no. 7, pp. 7976–7980, July 2020.
- [32] Y. Ge, Q. Deng, P. C. Ching, and Z. Ding, "OTFS signaling for uplink NOMA of heterogeneous mobility users," *IEEE Trans. Commun.*, vol. 69, no. 5, pp. 3147–3161, May 2021.
- [33] A. Bemani, G. Cuzzo, N. Ksairi, and M. Kountouris, "Affine frequency division multiplexing for next-generation wireless networks," in *ISWCS*, Berlin, Germany, 2021, pp. 1–6.
- [34] J. Zhu, Q. Luo, G. Chen, P. Xiao, and L. Xiao, "Design and performance analysis of index modulation empowered AFDM system," *IEEE Wireless Cmmun. Lett.*, 2023.
- [35] Y. Tao, M. Wen, and Y. Ge, "Affine frequency division multiplexing with index modulation," Sept. 2023. [Online]. Available: <https://arxiv.org/pdf/2310.05475.pdf>
- [36] L. Wu, S. Luo, D. Song, F. Yang, and R. Lin, "A message passing detection based affine frequency division multiplexing communication system," Aug. 2023. [Online]. Available: <https://arxiv.org/abs/2307.16109>
- [37] V. Savaux, "DFT-based modulation and demodulation for affine frequency division multiplexing," Aug. 2023. [Online]. Available: https://www.techrxiv.org/articles/preprint/DFT-Based_Modulation_and_Demodulation_for_Affine_Frequency_Division_Multiplexing/23804055
- [38] F. Kschischang, B. Frey, and H.-A. Loeliger, "Factor graphs and the sum-product algorithm," *IEEE Trans. Inf. Theory*, vol. 47, no. 2, pp. 498–519, Feb. 2001.
- [39] A. Bemani, N. Ksairi, and M. Kountouris, "AFDM: A full diversity next generation waveform for high mobility communications," in *2021 IEEE ICC Workshops*. Montreal, QC, Canada: IEEE, 2021, pp. 1–6.
- [40] Z. Liu and L.-L. Yang, "Sparse or dense: A comparative study of code-domain NOMA systems," *IEEE Trans. Wireless Commun.*, vol. 20, no. 8, pp. 4768–4780, Aug. 2021.
- [41] Q. Luo, Z. Liu, G. Chen, and P. Xiao, "Enhancing signal space diversity for SCMA over rayleigh fading channels," *IEEE Trans. Wireless Commun.*, Early Access, Sept. 2023.
- [42] L. Liu, S. Liang, and L. Ping, "On capacity optimality of OAMP: Beyond IID sensing matrices and Gaussian signaling," *IEEE Trans. Commun.*, Early Access, Sept. 2023.
- [43] Y. Chi, L. Liu, G. Song, Y. Li, Y. L. Guan, and C. Yuen, "Constrained capacity optimal generalized multi-user MIMO: A theoretical and practical framework," *IEEE Trans. Commun.*, vol. 70, no. 12, pp. 8086–8104, Dec. 2022.
- [44] J. Ma, L. Liu, X. Yuan, and L. Ping, "On orthogonal AMP in coded linear vector systems," *IEEE Trans. Wireless Commun.*, vol. 18, no. 12, pp. 5658–5672, Dec. 2019.
- [45] M. Tuchler, A. Singer, and R. Koetter, "Minimum mean squared error equalization using a priori information," *IEEE Trans. Signal Processing*, vol. 50, no. 3, pp. 673–683, 2002.
- [46] L. Liu, S. Huang, and B. M. Kurkoski, "Memory AMP," *IEEE Trans. Inf. Theory*, vol. 68, no. 12, pp. 8015–8039, Dec. 2022.
- [47] L. Liu, S. Liang, and L. Ping, "Capacity optimality of OAMP in coded large unitarily invariant systems," in *2022 IEEE ISIT*, Espoo, Finland, 2022, pp. 1384–1389.
- [48] "Evolved universal terrestrial radio access (E-UTRA); base station (BS) radio transmission and reception, 36.104, release 8." Apr. 24, 2021. [Online]. Available: https://www.3gpp.org/ftp/Specs/archive/36_series/36.104/
- [49] 3GPP TS 38.212, Rel. 15, "5G NR, multiplexing and channel coding," Jul. 2018. [Online]. Available: <https://www.etsi.org/deliver/etsits/138200138299/138212/15.02.0060/ts138212v150200p.pdf>